THESIS

GEOPHYSICAL CONSTRAINTS ON THE EVOLUTION OF AN EPHEMERAL CHANNEL AT THE SAND CREEK MASSACRE NATIONAL HISTORIC SITE, COLORADO, USA

Submitted by

Brad Sparks

Department of Geosciences

In partial fulfillment of the requirements

For the Degree of Master of Science

Colorado State University

Fort Collins, Colorado

Fall 2016

Master's Committee:

Advisor: Dennis Harry

Ellen Wohl
Peter Nelson

ABSTRACT

GEOPHYSICAL CONSTRAINTS ON THE EVOLUTION OF AN EPHEMERAL CHANNEL AT THE SAND CREEK MASSACRE NATIONAL HISTORIC SITE, COLORADO, USA

A geophysical survey was conducted on an ephemeral channel, Sand Creek, at Sand Creek Massacre National Historic Site to test three hypothesized migration and depositional models of ephemeral streams. A key motivation for the study is to identify the historical location of Sand Creek, which is critical to establishing the location of the 1864 Sand Creek Massacre. Hammer seismic refraction data were collected on 7 valley-wide lines oriented perpendicular to the channel, and ground penetrating radar data (200 MHz antenna) was collected on a grid overlying the channel and the channel banks. An additional GPR line (100 MHz) was collected on a line spanning the valley bottom. The refraction data show 4 layers: an eolian cap that is 1 - 3 m thick with a velocity of 0.3 km/s; a gradational alluvium layer consisting of ephemeral deposits which is 2 – 3 m thick with velocities ranging from 0.5 - 1 km/s; a gradational alluvium layer consisting of perennial fluvial deposits which is 2 - 7 m thick with velocities ranging from 1.2 - 2.9 km/s; and a homogeneous layer with a velocity of 2.4 km/s which is interpreted to be the Pierre Shale Formation. The radar data located buried channel boundaries and revealed a change in bedforms at 3 - 4 m deep. The change in bedforms is interpreted to indicate a flow regime change from an older perennial to a more recent ephemeral flow. The channel bedforms within the ephemeral flow regime deposits suggest that the channel has not migrated across the modern valley since the ephemeral flow regime was established, but punctuated changes in morphology within the channel have occurred in association with major floods. The results

indicate that the channel has not changed position in historical times. This suggests that the modern stream is the proper geographic context for historical accounts that reference the location of Sand Creek when describing events that occurred during the 1864 massacre.

ACKNOWLEDGEMENTS

Many thanks to the National Park Service and the Sand Creek National Park staff, and specifically Karl Zimmerman. Their support and assistance in the field and during my research was paramount to the completion of this project.

I also cannot say enough on behalf of my advisor Dennis Harry, and my committee members, Ellen Wohl and Peter Nelson. I was much more equipped to do successful research because of their input and I am more suited to proceed into the rest of my career because of their wisdom in their fields of science.

I would be remiss if I did not thank the 2016 World Series Winners - the Chicago Cubs. Their incredible and historic season provided me with hope and encouragement as I finished this project.

Lastly, I would like to thank my wife Libby as she journeyed with me out to Colorado to create a new home for our family as I endeavored to further my knowledge in Geophysics. I would not have been able to start or finish my research without her always by my side.

DEDICATION

I dedicate this research to the Native American victims and their families of the Sand Creek Massacre. I hope that through my work they can gain some clarity about the horrific events that occurred to them on November 29, 1864.

TABLE OF CONTENTS

CHAPTER 1: INTRODUTION AND THE SAND CREEK MASSACRE

Introduction

This thesis describes a geophysical study conducted at the Sand Creek National Historic Site. Sand Creek was the site of the Sand Creek Massacre (described below). One motivation of the study is to determine the location of Sand Creek at the time of the massacre. Another is to learn more about ephemeral streams.

The primary results of this research are reported in Chapter 2, which has been formatted for submittal as a journal article to The Mountain Geologist. Chapter 3 contains a full description of the data used in this research. Chapter 4 contains recommendations for future research.

The Massacre

The information below was taken from *Sand Creek Massacre Project: Site Location Study, Volume 1* (National Park Service, 2000). For further information regarding the massacre events, the legislative mandate to locate the massacre, and additional documents pertaining to the massacre refer to *Sand Creek Massacre Project: Site Location Study*.

The Sand Creek Massacre occurred on November 29, 1864 along the banks of the Big Sandy Creek in Kiowa County, Colorado (Big Sandy Creek is commonly referred to as Sand Creek). Colonel John Chivington led a group of approximately 700 soldiers from Fort Lyons through an overnight ride 40 miles to the banks of the "Big Sandy". Members of the Cheyenne and Arapaho tribes were encamped at that location, assuming U.S. protection, after being instructed to do so by Colorado Governor John Evans after they approached Fort Lyons to receive provisions and protection before returning to their designated lands as established by the 1861 Treaty of Fort Wise. Due to the passive intentions of the Cheyenne and Arapaho, their encampment was composed mainly of elderly, woman, and children.

At dawn, the soldiers struck the native encampment with cavalry and at least two 12-pounder mountain howitzers. As chaos ensued, the Cheyenne and Arapaho fled northward and also sought shelter in rapidly dug out trenches, referred to as the "Sandpits." By the end of the violence, at least 150 Cheyenne and Arapaho were killed. Chivington and his troops returned to Denver as "heroes" but were soon recognized as committing a national disgrace and condemned by two congressional committees and a military commission.

Massacre Site In Question

Due to the chaotic and sudden nature of the massacre, oral histories, written documents, and hand drawn figures from Chivington troops and the Cheyenne and Arapaho contradict each other on the exact location of the massacre. In 1950, the Colorado Historical Society erected a historical marker denoting the site of the massacre along Colorado State Highway 96. That same day the Colorado Historical Society participated in another dedication ceremony in an area that overlooked the "Dawson Bend" area of Sand Creek. In that same area a marker designating the massacre site was placed by local residents, the Colorado Arkansas Valley Inc., and the Eads and Lamar Chambers of Commerce. In 1978, the Arrow Keeper of the Cheyenne Tribe blessed this same area as "Cheyenne Earth."

The multiple massacre site designations led to the introduction of Senate Bill 1695 by Colorado Senator Ben Nighthorse Campbell. On October 6, 1998, after passing through the Senate and the House of Representatives, President Bill Clinton signed the bill as Public Law 105-243. Public Law 105-243 directed the National Park Service to "identify the location and extent of the massacre area and the suitability and feasibility of designating the site as a unit of the National Park Service System." Since 1999, the National Park Service has been conducting research to fulfill this mandate.

Purpose of This Study

To locate the old Sand Creek and to learn more about ephemeral streams.

References

National Park Service, 2000, Denver, Intermountain region. Sand Creek Massacre Project, Site Location Study, v.1:.

CHAPTER 2: GEOPHYSICAL RESEARCH AT SAND CREEK MASSACRE NATIONAL HISTORIC SITE

Introduction

Ephemeral streams flow episodically throughout the year and are dependent on local rainfall to provide surface flow. Their dependence on unpredictable, high intensity rainfall in the immediate vicinity of the stream makes it challenging to measure or observe depositional patterns created during channel migration. Standard geomorphological techniques such as tree coring, soil sampling, and remote sensing provide only limited insight into channel history and associated depositional patterns. Coring cottonwood trees that grow along ephemeral stream banks can constrain the ages of floods, for example, because cottonwoods germinate in overbank flood deposits, but tree cores do not record sediment deposition patterns and cover less than circa 200 years of time. Soil samples provide accurate and detailed sediment data, but samples are commonly collected from widely spaced locations and require interpolation over large areas. Because ephemeral streams are characterized by substantial spatial variability, interpolation of sparse data creates a large amount of uncertainty. Remote sensing provides spatially dense data, but the data are constrained to the most recent depositional events recorded in surficial deposits, and do not necessarily capture previous depositional events. All of these methods provide valuable data that can be extrapolated to predict migration patterns of more predictable, perennial channels, but a more robust method is needed for measuring migration patterns of ephemeral streams.

Various geophysical methods have proven useful in surveying perennial fluvial systems. Ground penetrating radar (GPR) has been shown to be capable of imaging paleofluvial sediments in order to determine the location and dynamics of paleo channels (Vandenberghe and

Overmeeren, 1999). Detailed imaging of bar-scale (Bridge et al., 1998) and channel-scale sedimentary structures (Skelly et al., 2003) has been conducted using GPR to map the architecture of braided channel systems. GPR has been used to image meandering channel systems to identify their migration patterns (Wooldridge, 2005; Słowik, 2011). Seismic refraction has shown utility in distinguishing fluvial from non-fluvial deposits on the basis of differences in p-wave velocities as well as layer thicknesses (Schrott and Sass, 2008). Resistivity has been used to locate buried paleo channels by distinguishing clay-rich over bank deposits from coarse channel fill deposits (Sinha et al., 2013). Because different geophysical methods measure different aspects of fluvial deposits, application of multiple geophysical methods to the same problem is most useful for understanding fluvial systems (Hirsch et al., 2004).

The studies cited above show that geophysical methods, particularly GPR and seismic refraction, can be used to produce images of the subsurface geology that greatly improve our understanding of perennial fluvial systems and processes. However, relatively little geophysical work has been applied to understanding the evolution of ephemeral stream migration. Ephemeral streams commonly occupy wide valley bottoms compared to the dimensions of the active channel. Due to the inconsistency of surface flow, it is unclear if individual ephemeral channels migrate relatively continuously across these drainages, migrate across the valley via frequent jumps to random positions, or are quasi stable with relatively little change in channel location. In this study, GPR and seismic refraction data were collected to constrain sedimentation patterns and stream dynamics in an ephemeral stream on the central North American High Plains in eastern Colorado, USA. Sedimentation patterns inferred from the geophysical data are used to test models of ephemeral stream evolution. Continuous stream migration should produce a vertically and laterally gradational facies change with systematically stacked, laterally offset

channels. Stream migration by distinct jumps in the channel position is expected to be associated with multiple, spatially distinct, and possibly cross-cutting channels. Relatively few buried channels indicate quasi stable channel systems.

The observed sedimentation patterns and stream dynamics will be used to identify a migrational model for ephemeral streams and applied to solving a historical problem tied to the study site. The study was conducted at the Sand Creek Massacre National Historic Site, which is the location of the Sand Creek Massacre. In 1864, approximately 150 Native Americans were killed by US troops along the banks of Sand Creek. However, the location of Sand Creek at the time of the massacre is in question as it may have migrated since 1864, leaving in question the location of the massacre. This study investigates the historical mobility of Sand Creek, providing new constraints on the location of Sand Creek at the time of the Sand Creek Massacre.

Ephemeral Streams and Sand Creek

Dryland channels vary greatly from perennial channels in humid regions. Because of their location, dryland channels are typically ephemeral and rely on localized high intensity and infrequent floods for surface flow, sediment transport, and channel morphology (Graf, 1988; Tooth, 2013). Perennial channels have water supply in headwaters farther upstream that flow downslope in a single, well-bounded channel. This leads to reliable flow with transmission losses mainly due to evaporation. Hydrographs for perennial channels are broad based following precipitation, and these channels return to an equilibrium flow state after high flows occur (Tooth, 2013). In contrast, water supply for ephemeral channels is dependent on localized high intensity and infrequent floods. Because of these floods, ephemeral channels are disconnected from other channels in the drainage network. Flow transmission losses are due mainly to seepage in the unconstrained alluvium in the channel bed. The unconstrained alluvium generally provides

a lot of sediment supply during floods, leading to spatially variable bedforms (the term "bedforms" is being used to describe any depositional or structural features of channels) within the channel. Depending on the amount of vegetation, ephemeral channels can undergo high amounts of channel change during floods and typically do not have a state of equilibrium flow.

While generalized theory regarding perennial channels exists, ephemeral stream environments are too varied to have accurate generalized theory (Tooth, 2013).This is due to various factors such as aridity, tectonics, structure, slope-channel coupling, lithology, and vegetation that change for each ephemeral catchment (Tooth, 2013). These factors lead to differing channel slopes, flow velocities, bedforms, and channel morphology. It would be extraneous to describe all the studied ephemeral stream environments, but it is useful to give context for the ephemeral stream environment at Sand Creek. From field observations it can be concluded that Sand Creek is a braided ephemeral channel (Graf, 1988), as seen by the deposits of sand and gravel, various in-stream bars, and small, cottonwood-lined sub channels. The channel and channel bank slopes are not at a steep gradient, less than 2%. This limits maximum flow velocities and sediment supply from floods, which reduces the amount of erosion, sedimentation, and changes in channel morphology that occur. However, at Sand Creek, sedimentation does occur in the channel and the flood plain because of high amounts of vegetation on the usually dry channel bed and channel banks (Graf, 1988). The vegetated channel bed helps to limit channel incision and create a wide, shallow cross-sectional geometry.

Geological and Historical Setting of Sand Creek

The research site lies along a stretch of Sand Creek that is located at Sand Creek Massacre National Historic Site in Kiowa County in southeastern Colorado, USA (Figure 1). Sand Creek is a High Plains ephemeral stream and a tributary of the Arkansas River. The

headwaters of Sand Creek are located in the Front Range of the Rocky Mountains in El Paso County, Colorado, although localized floods control the regional flow. The geology of the Sand Creek valley is described by a ground water resource assessment conducted by the United States Geological Survey (USGS) (Coffin and Horr, 1967). Holocene and Pleistocene eolian sands overlie most of the area, and can be up to 20 m thick outside of the valley. Underlying the eolian sands are Holocene and Pleistocene valley-fill deposits that range from clay to gravel size sediments, but generally coarsen downwards and can be up to 20 m thick. Along the northern edge of the valley are Pleistocene upland deposits composed of sand and gravel with caliche stringers. The upland deposits are up to 10 m thick. The Cretaceous Pierre Shale Formation underlies the Quaternary deposits and is in excess of 1000 m thick.

This particular stretch of Sand Creek is part of a sharp bend at which the creek changes from a southerly flow to an easterly flow (Figure 2). At this location, the stream lies within a valley that strikes northwest and is bounded by bluffs and eolian dunes approximately 5 m high along its southern edge. A continuous eolian dune borders the northern edge of the valley (2000 m in length) and gradually rises to approximately 10 m above the valley floor. The valley fill is composed of gravel, sand, silt, and clay, varying from 2-15 m thick (Coffin and Horr, 1967). Relief in the valley is less than 0.5 m, except in the active channel. The active channel is situated along the southern edge of the valley and varies from 1 to 5 m in width, containing up to 1.5 m of relief relative to the rest of the valley floor. The vegetation in the valley is predominantly sage brush and buffalo grass with prairie grasses also occupying the channel bed. The channel is lined by a gallery of cottonwood trees.

Surface flow within the active channel is infrequent and only occurs after extreme precipitation (Karl Zimmerman, U. S. Park Service, May 2015, personal communication). For

example, the peak discharge on May 4,1999 was 2850 cfs (80.7 $m^3 s^{-1}$), with a gage height of 9.65 ft (2.94 m) (USGS, 2005). From the available data, which date from 1968 – 2005, the average monthly flow for Sand Creek at this location varies from 166 cfs (4.70 $m^3 s^{-1}$) in May of 1999 to 0.73 cfs (0.02 $m^3 s^{-1}$) in October 2003 (USGS, 2005). The average precipitation for June – September is 7.80 inches (0.198 m), with an average temperature of 71.29 °F (21.83 °C). For October – May, the average precipitation is 14.72 inches (0.374 m), with an average temperature of 42.59°F (5.88°C) (ESRL, 2005).

The location of the Sand Creek channel during the past two centuries is of interest due to the historical significance of the stream. The Sand Creek Massacre occurred at the site on November 29, 1864 as 700 US soldiers and militia men attacked and killed approximately 150 Native Americans encamped along the banks of Sand Creek. Oral and written records document the massacre as happening along the northern banks of Sand Creek. However, due to the dynamic nature of ephemeral stream systems, the actual location of Sand Creek in 1864, and thus the location of the massacre, is uncertain (National Park Service, 2000). Three surficial studies have been conducted to locate the 1864 channel using different methods. Geoarchaeological surveys locating anthropogenic artifacts along stream terraces (Holmes and Mcfaul, 1999), tree stand ages (Lukas and Woodhouse, 2006), and hydrological and geomorphological records (Martin et al., 2013) have all indicated the stream has not changed position since the massacre. However, these data mostly address the modern stream deposits, which may be younger than 1864. Accordingly, the prior studies lack sufficient data to make a definitive conclusion regarding the position of the stream at the time of the massacre or the frequency and nature of changes in channel position through time.

Figure 1. Sand Creek at Sand Creek Massacre National Historic Site in southeastern Colorado.

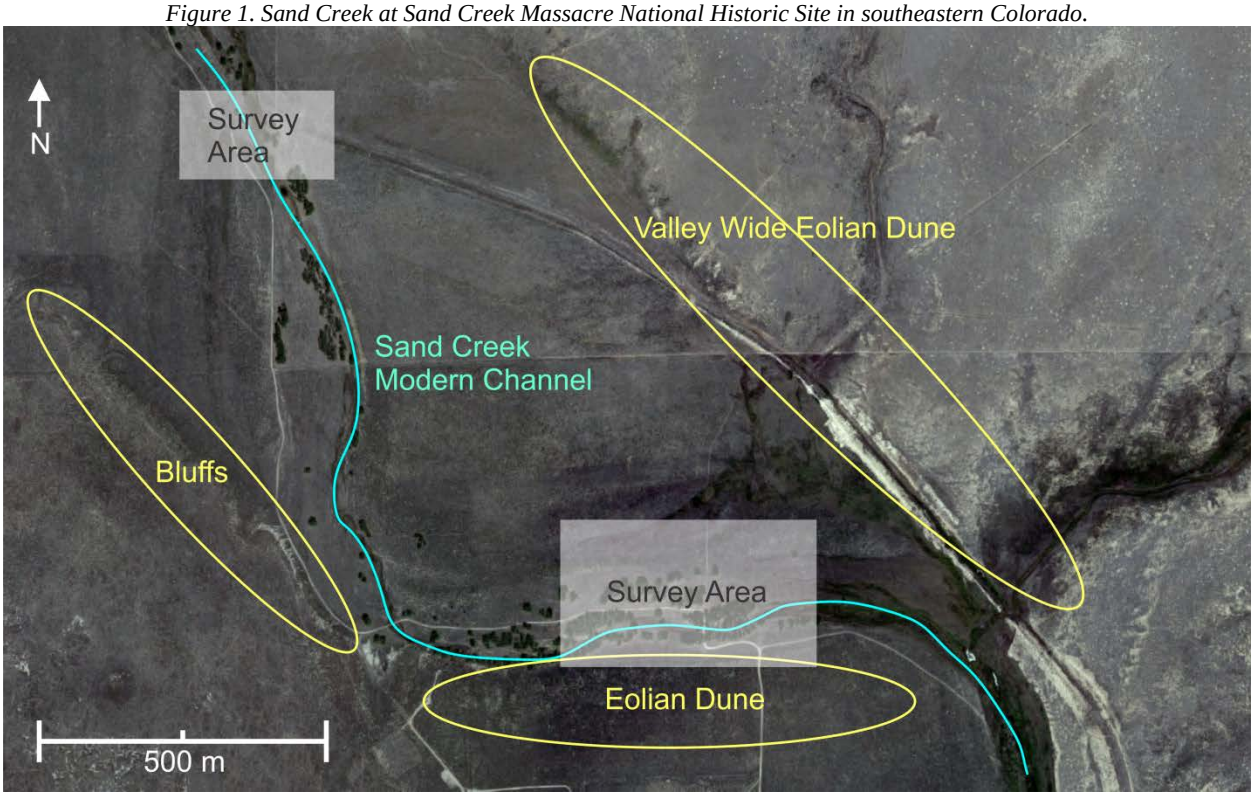

Figure 2. Aerial photograph of the stretch of Sand Creek surveyed in this study. The valley is bounded by a continuous eolian dune to the northeast and bluffs and dunes to the south and west. Photo from Google Earth.

Methods

Basic Refraction and GPR Concepts

For near-surface applications, seismic refraction and ground penetrating radar (GPR) are particularly useful geophysical tools. Seismic refraction uses a seismic source to generate a seismic wave that propagates through the subsurface. The waves are refracted when they pass through layers or regions of different velocity. The travel time of refracted arrivals can be used to build a model of the subsurface velocity structure. Layered velocity models can be generated using head waves, which are refracted at interfaces that have a higher velocity beneath. In seismic tomography, all refracted arrivals are used (not just the head wave), allowing for a model with gradational lateral and vertical velocity changes. Seismic refraction is useful for imaging layers of different lithology and identifying lateral and vertical velocity variations between and within each layer.

GPR transmits polarized electromagnetic waves into the ground that reflect back to the system receiver. The reflections are produced at interfaces separating materials of different dielectric constants. Dielectric constants vary with subsurface material based on the composition, grain size and sorting, porosity, and pore saturation of that material. As a result, any object or layer in the subsurface that is composed of different materials will produce a reflection on a GPR profile. Stronger reflections are a result of higher contrasts in dielectric constants between material boundaries. GPR is useful for identifying stratigraphic layering in the subsurface, and stratiforms within the layers.

Survey Setup

Seismic refraction and GPR profiles were collected on a south-flowing segment of the creek located upstream of the bend in the channel, and on an east-flowing segment located

downstream of the bend (Figure 3). The upstream (south-flowing segment) survey consisted of three lines oriented perpendicular to the channel (Lines UP1, UP2, and UP3). The upstream lines were collected to determine the subsurface structure of the area just upstream and just downstream of an irrigation canal that was dug in the 1930's. That area has been hypothesized as an alternate location of Sand Creek in 1864 (National Park Service, 2000). UP1 is 186 m long and spans the modern channel and the area just upstream of the old canal gates. UP2 is 138 m long and spans the old canal and the area bounding the canal just downstream of the old canal gates. UP3 is 92 m and spans the canal farther downstream of UP2. The downstream (east-flowing segment) survey consisted of three lines oriented perpendicular to the channel (Lines 1, 2, and 3) and one parallel to the channel (Tie Line). The downstream survey was collected to determine channel position changes within the valley. Line 1, located farthest downstream, is 396 m long and spans the entire width of the valley. Line 1 was collected in order to determine the number and position of buried paleo-channels within the valley. Lines 2 and 3 are 186 m long, and focus primarily on identifying migration patterns in the modern channel system and characterizing stream-parallel variability. A GPR grid with higher spatial resolution was collected in the area bounded by refraction Lines 2 and 3 in order to get a detailed picture of the depositional patterns within and surrounding the active channel. The grid dimensions are 10 m (north-south) by 15 m (east-west), with six lines running parallel to the channel and five lines running perpendicular to the channel (GPR grid lines are referred to as GL #). Elevation surveys were conducted at 10 m intervals (unless significant relief was present, in which case readings were taken at the start, inflection point, and end of the relief) using a TruPulse 360B laser rangefinder for every refraction line. Elevations were measured relative to informal benchmarks at the starting point of each line to determine elevation change along the lines.

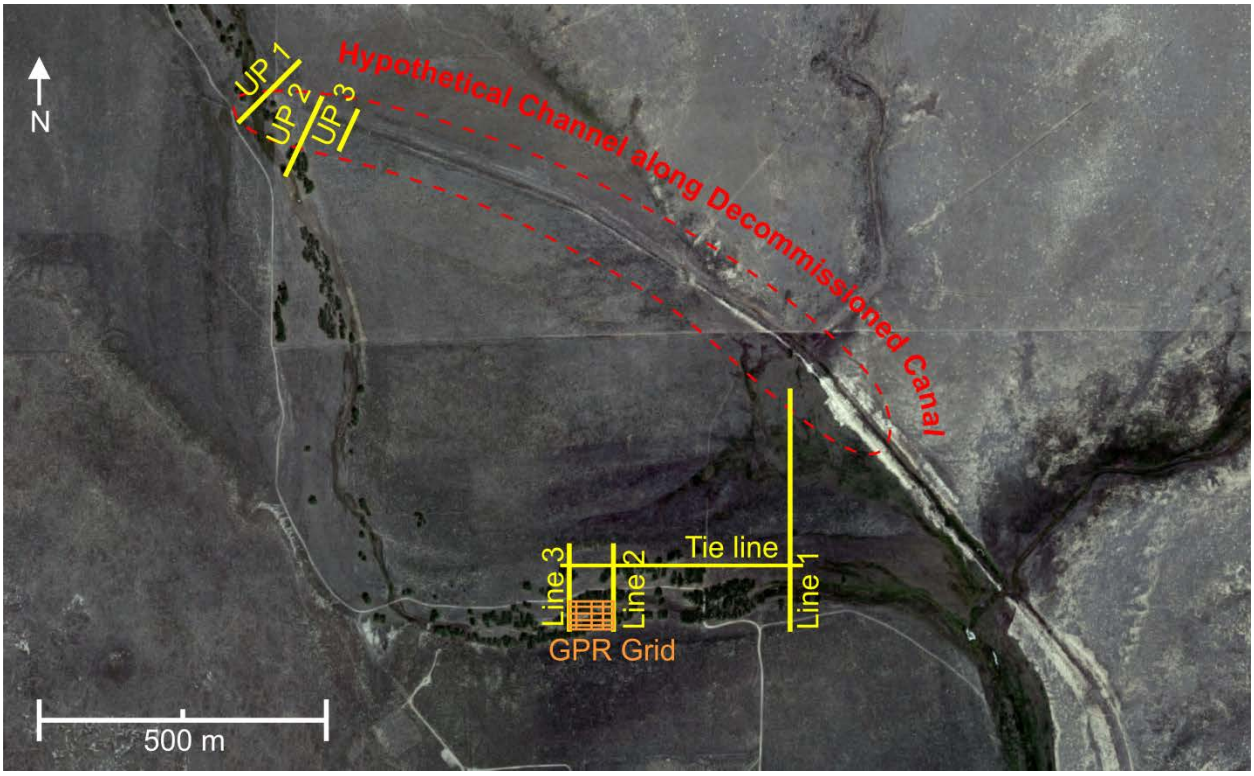

Figure 3. Survey lines and grid for the seismic and GPR data. One hypothesized location of the 1864 channel is the area near the irrigation canal, outlined in red.

Seismic Methods

For the seismic refraction surveys, a 16 pound sledgehammer was used as the seismic source. Data were recorded with a 24 channel Geometrics Geode system with 14 Hz vertical component geophones spaced every 2 m. Shots were stacked 3 times and collected at 0 m, 6 m, and 12 m offsets from the first geophone at each end of the line segment. The line segments were leapfrogged to create a full line, with the first geophone of a line segment starting at the farthest offset from the last geophone of the previous line segment.

The refraction data were processed using the Seisimager software package by Geometrics. The first arrivals for the refraction surveys were identified in the PickWin program of the Seisimager package (Figure 4). After all of the first breaks are picked for each shot on a line, the travel time curves are generated for the whole line (Figure 5). The first arrival times were then imported into the PlotRefa software to create an initial, 2-layer velocity model via a

time term inversion (Figure 6). The time term inversion computes a best linear least squares fit to the delay-time of the head wave first breaks. The delay-time is the difference between the observed arrival time and the predicted arrival time for a model with planar interface. The program adjusts the topography on the interface (simultaneously solving for layer velocities) to create the final layered velocity model ("SeisImager Manual," 2009). The 2-layer model is simplistic, as it treats all first arrivals as if generated by a head wave at the layer interface and assumes constant velocity within each layer. To achieve a more realistic model, a more robust tomographic inversion was done (Figure 7). The 2-layer velocity model from the delay-time inversion was used as an initial model for the tomographic inversion. The tomographic inversion traces rays through the velocity model, iteratively adjusting the velocity to minimize the root mean square (RMS) error between the observed and calculated travel times. Raypath travel times are computed by breaking up the initial model into a grid and summing the raypath travel time through each grid cell. The travel path of the ray is computed with Snell's Law, which governs refraction at cell boundaries. In the tomographic method, the velocities in each cell are adjusted iteratively to minimize the misfit between the modeled and observed travel times ("SeisImager Manual," 2009). The tomographic inversion provides a more realistic velocity model than layered inversion methods in fluvial systems, as it can resolve gradational and lateral velocity changes. The grid used for the tomography models extends to a maximum depth of 40 m with 15 grid layers and a grid cell width of 1 m (half the geophone spacing). Minimum and maximum allowable velocities were set to 200 m/s and 3000 m/s, respectively. The inversion was weighted to slightly smooth the velocity changes equally in the vertical and horizontal directions. For lines with significant topographic relief, the inversion was weighted slightly more for horizontal smoothing to minimize any topography artifacts in the inversion. The tomographic inversions

achieved a large reduction in the model misfit in the first three iterations. Further iterations resulted in only modest reductions in the misfit and added significant variance (small-scale heterogeneity) to the model. The geological interpretation is based on the third iteration, which is the simplest of the best-fitting models. Accordingly, in all figures showing a tomographic inversion, the third iteration is displayed.

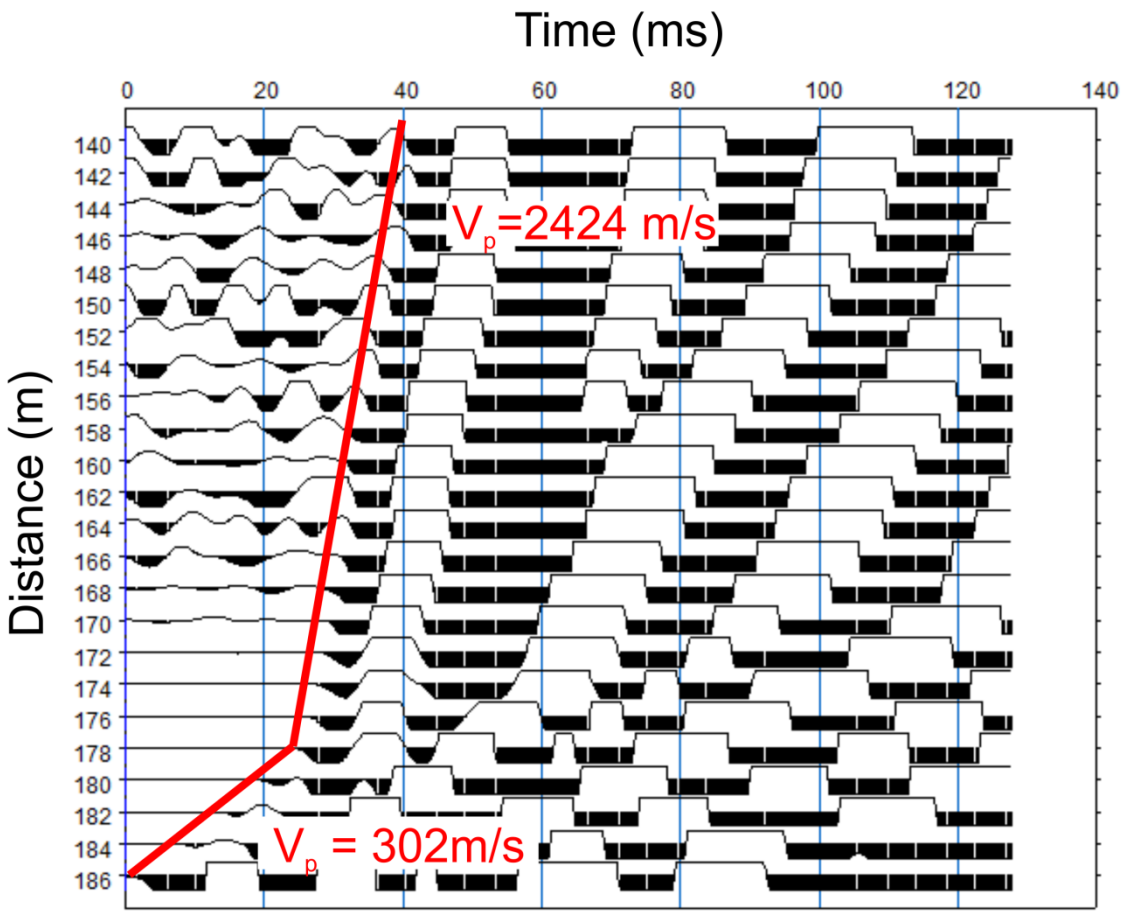

Figure 4. Shot record for a shot along Line 1. This is typical of the data quality for all of the seismic lines. First arrivals indicate two layers, with their corresponding layer velocities shown in red.

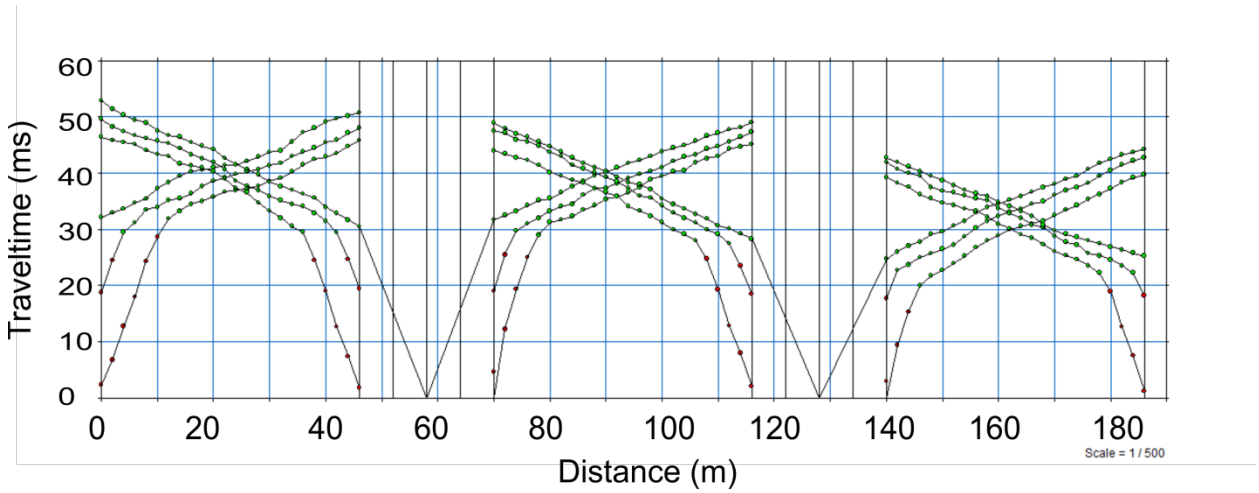

Figure 5. Travel time curves for seismic refraction line UP1. Red dots indicate arrivals attributed to the top layer. Green dots are arrivals attributed to the second layer.

.

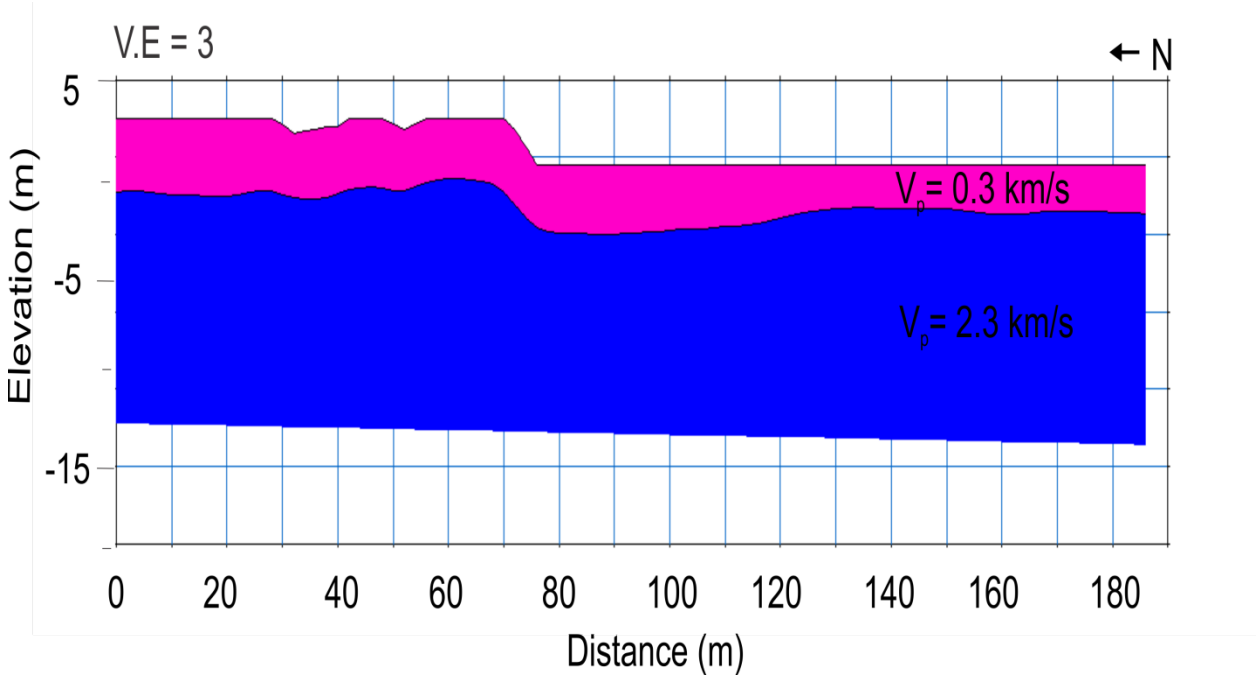

Figure 6. Two layer velocity model for UP1 generated using a time-term inversion and the travel time curves in Figure 5. RMS error of 0.39 ms.

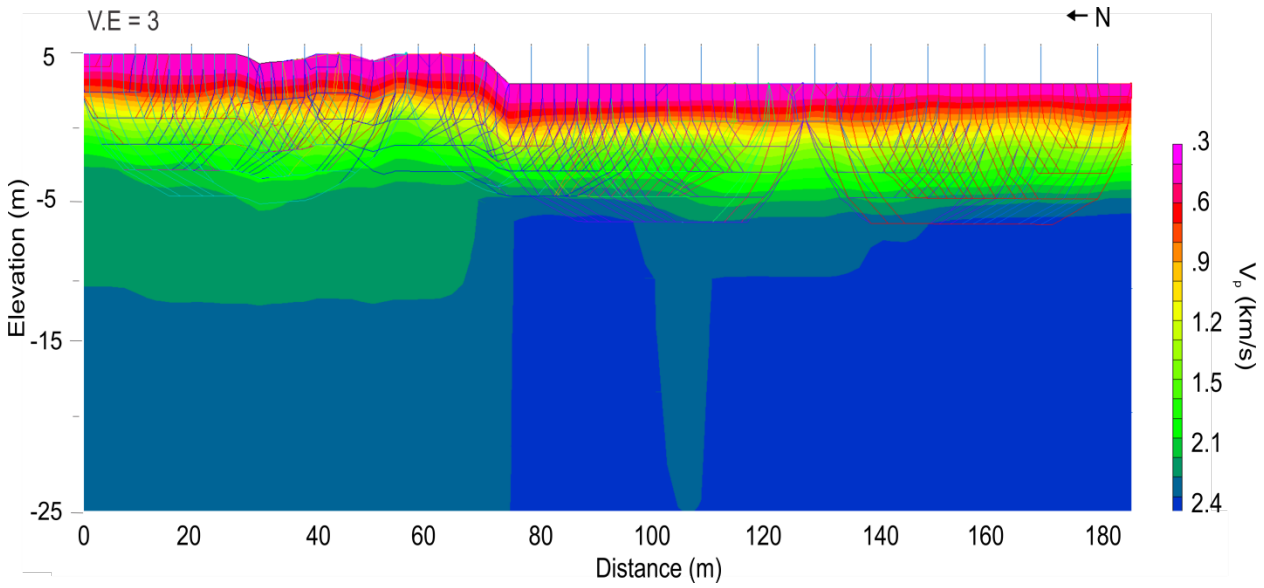

Figure 7. Tomographic model of UP1 generated with the two layer velocity model as an initial model. The raypaths indicate model sensitivity, showing that the subsurface is interrogated well down to the top of the high velocity layer at relative depths of 6-8 m. RMS error of 1.33 ms.

GPR Methods

The GPR data were collected using a Sensors and Software Pulse Ekko Pro system. Antenna center frequencies were 200 MHz for the grid and 100 MHz for the line. The grid data were collected using a 0.1 m step size, while the line was 0.2 m step size. The sampling interval was 0.83 ns for the 200 MHz antennas and 1.67 ns for the 100 MHz antennas. The antenna were oriented parallel to the survey with a separation of one antenna length (0.125 m for the 200 MHz antennas and 0.25 m for the 100 MHz antennas). Each GPR record was collected over a 200 ns time window and the signal was stacked 4 times. The GPR profiles are topographically corrected and repositioned prior to processing. The grid profiles show strong reflections to average travel times of 25-35 ns (Figure 8). The GPR grid lines are numbered from GL 2-12 (Figure 9).

The raw GPR data (Figure 10) were processed with Ekko View Deluxe by Sensors and Software. An Automatic Gain Control (AGC) gain with a maximum (multiplicative) gain of 150 and a window width of 0.5 pulses was applied to each line to amplify reflections throughout the GPR profile (Figure 11). Another version of the GPR lines was created with a Spherical and

Exponential (SEC) gain correction, using a maximum (multiplicative) gain factor of 500 and an exponential attenuation factor of 2.5 (Figure 12). The SEC gain preserves relative amplitude changes, so that differences in the amplitude of the reflections indicate differences in the magnitude of the dielectric permeability contrast. For the grid lines, a low pass filter was applied with a cutoff of 250 MHz to remove background noise. Diffractions were identified and were used to calibrate a velocity model for each line (Figure 13). The calibrated velocity model for all of the GPR lines was 0.1 m ns $^{-1}$.

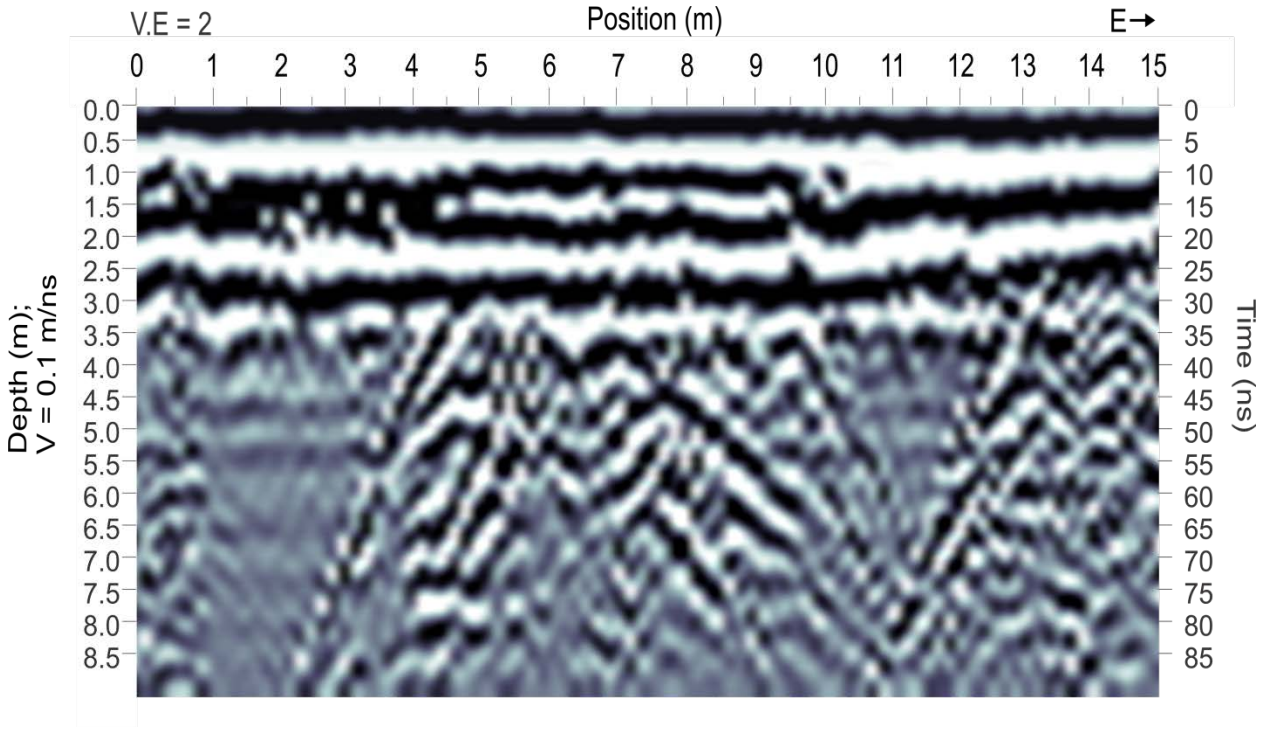

Figure 8. Example of the data quality for the GPR grid lines using 200 MHz antennas. Depth is based on a velocity of 0.1 m/ns, as discussed in the text.

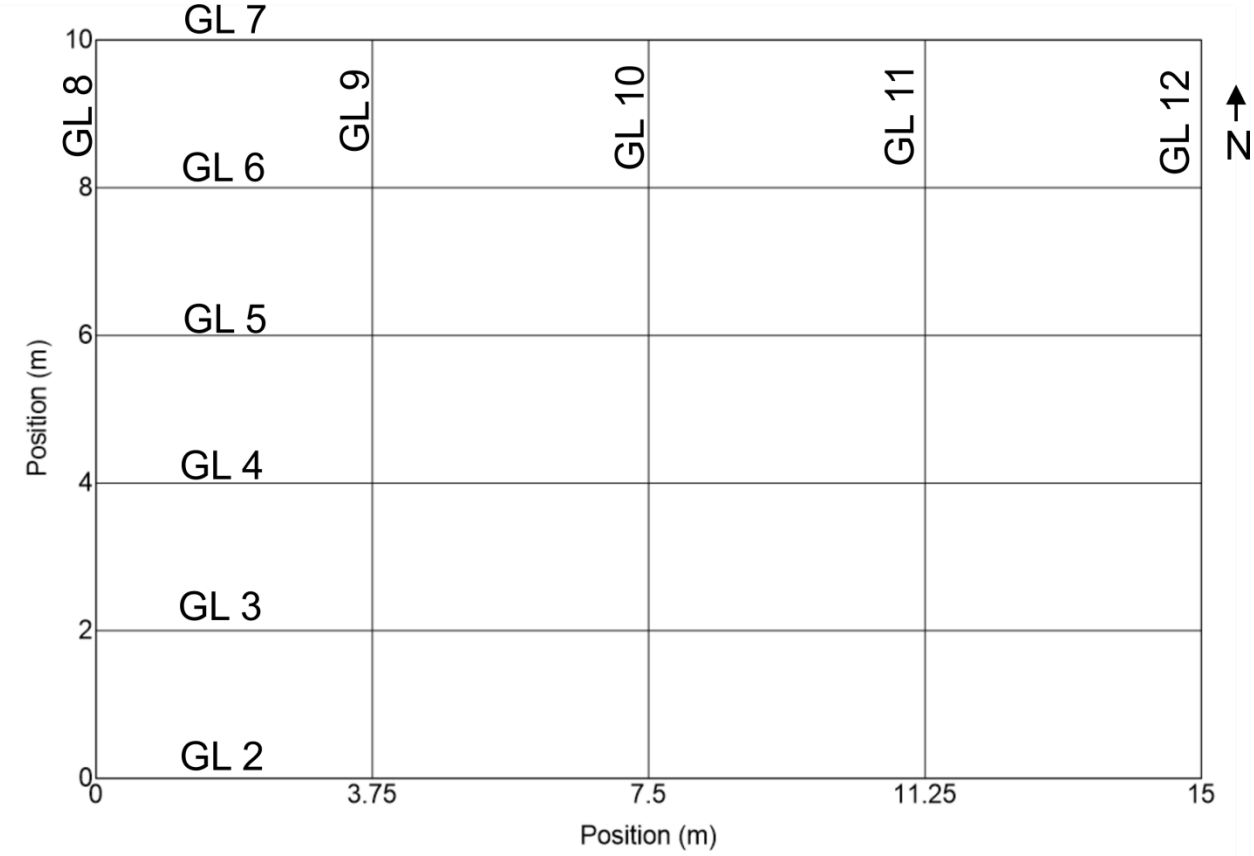

Figure 9. Layout and numbering for the GPR grid.

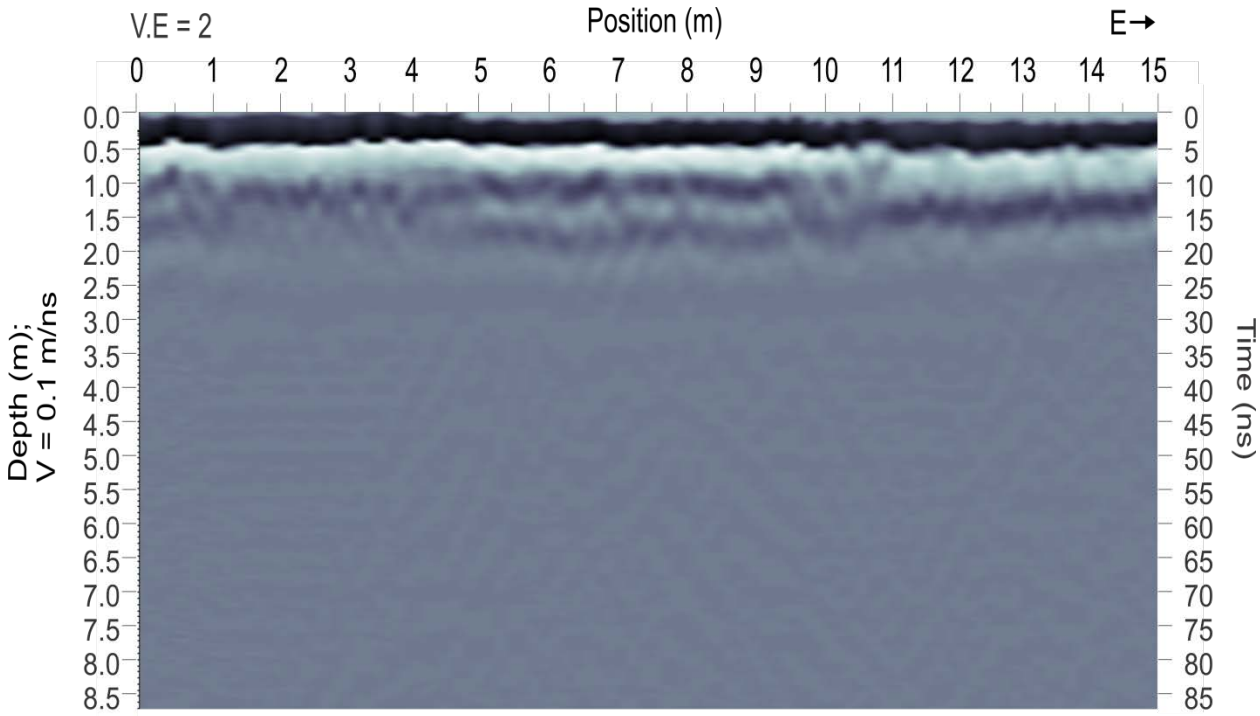

Figure 10. Example of unprocessed GPR data. Depth is based on a velocity of 0.1 m/ns, as discussed in the text.

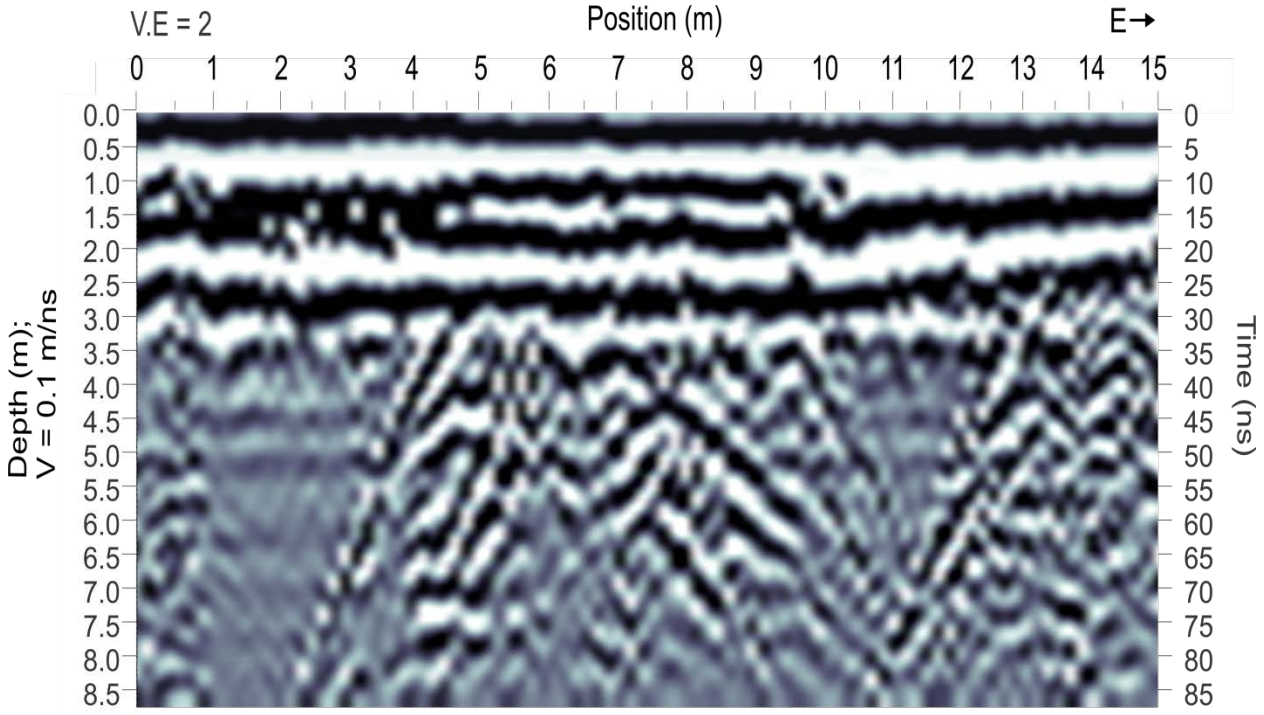

Figure 11. Example of an AGC gained GPR profile. Depth is based on a velocity of 0.1 m/ns, as discussed in the text.

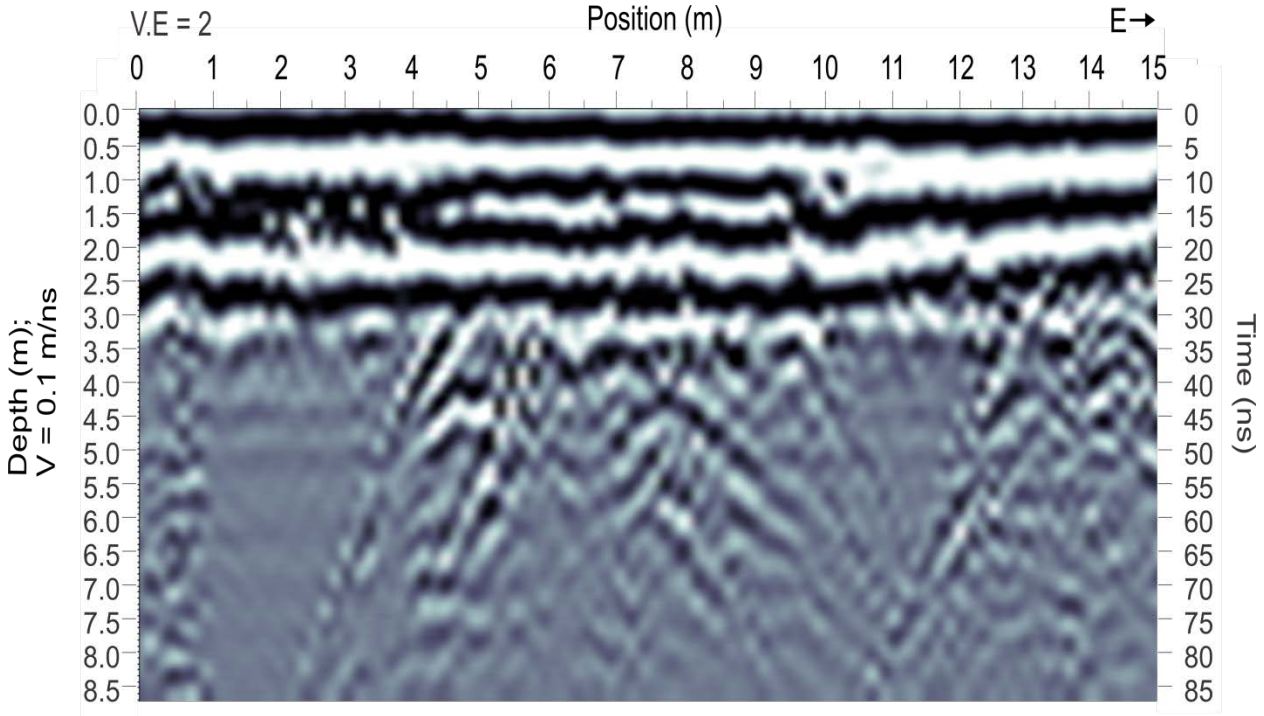

Figure 12. Example of an SEC gained GPR profile. Depth is based on a velocity of 0.1 m/ns, as discussed in the text.

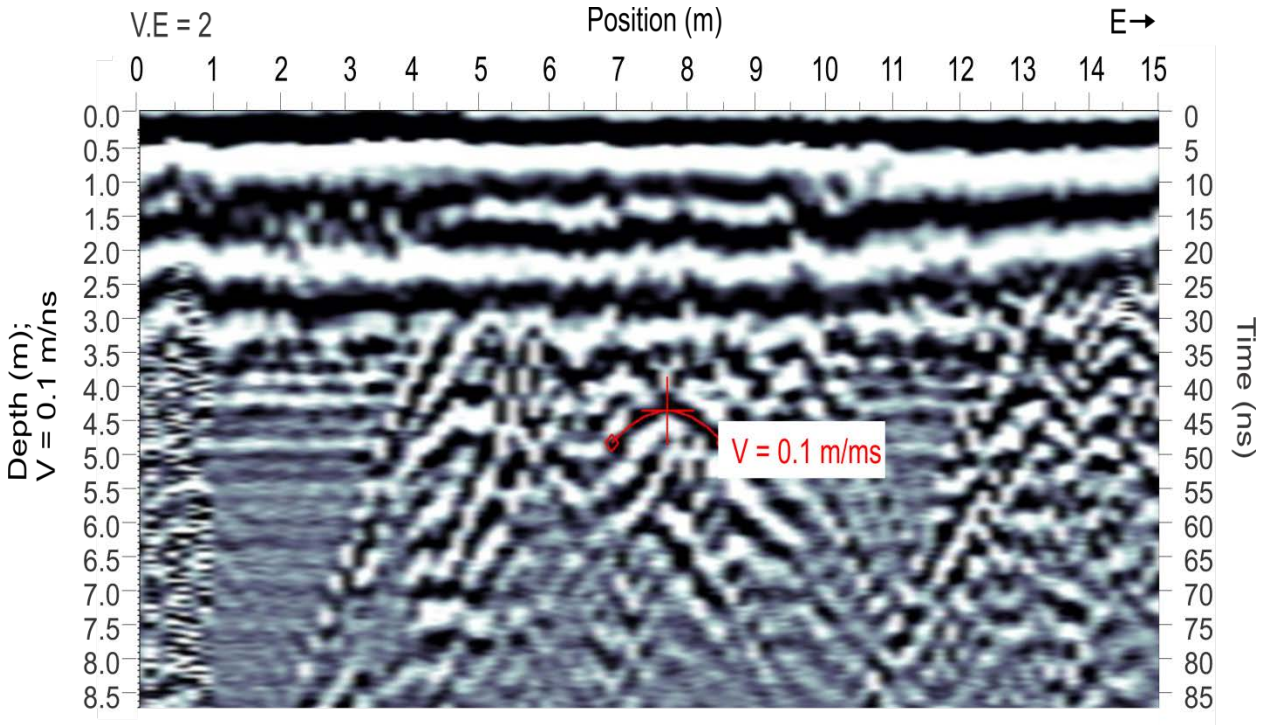

Figure 13. Velocity calibration using a diffraction on GPR grid line GL 2. A velocity of 0.1 m/ns was used for all GL as a result of the diffraction calibrations. Depth is based on a velocity of 0.1 m/ns, as discussed in the text.

Results

Refraction Results

The seismic refraction tomographic profiles show a four-layer velocity structure with two discrete layers of near-uniform velocity bounding two layers with vertically gradational velocities (Figures 15-17). The uppermost layer, S1, has a velocity of approximately 0.3 km/s (pink in the tomography profiles) and typically is 1 – 3 m thick, but at some places can be non-existent. This is underlain by a steep velocity gradient layer, S2, in which velocity decreases downward from around 0.5 to 1 km/s (red/yellow in the tomography profiles). S2 is usually 2 – 3 m thick. The second gradational layer, S3, has a lower velocity gradient, with velocity increasing from 1.2 to 2 km/s (greens in the topography profile). S3 varies much more in thickness than the other layers, usually ranging from 2 – 7 m thick. The final layer, S4, has a nearly uniform

velocity of 2.4 km/s (blue in the tomography profile). The thickness of S4 is not constrained by the refraction data and is cut off for display purposes.

Layer S1 appears to be non-existent in places with prominent topography, such as at 100 m and 130 m on Line 3 (Figure 15) and 105-135 m on UP2 (Figure 17). In most areas, however, S1 is of nearly uniform thickness, draping over topographic relief. There are also numerous areas where the top of S4 has relatively large topographic depressions. This is observed on Line 1 at 50, 150, and 200 m (Figure 15), and on Line 3 around 35 m and again from 70 – 180 m (Figure 16). Line 1, Line 3 and UP2 all display similar features. However, the topography feature on the south side of UP2 (Figure 17) is not considered to be realistic as it does not show up on the line or the shot record before a topographic correction is made. Therefore, it is concluded to be an artifact created by the software.

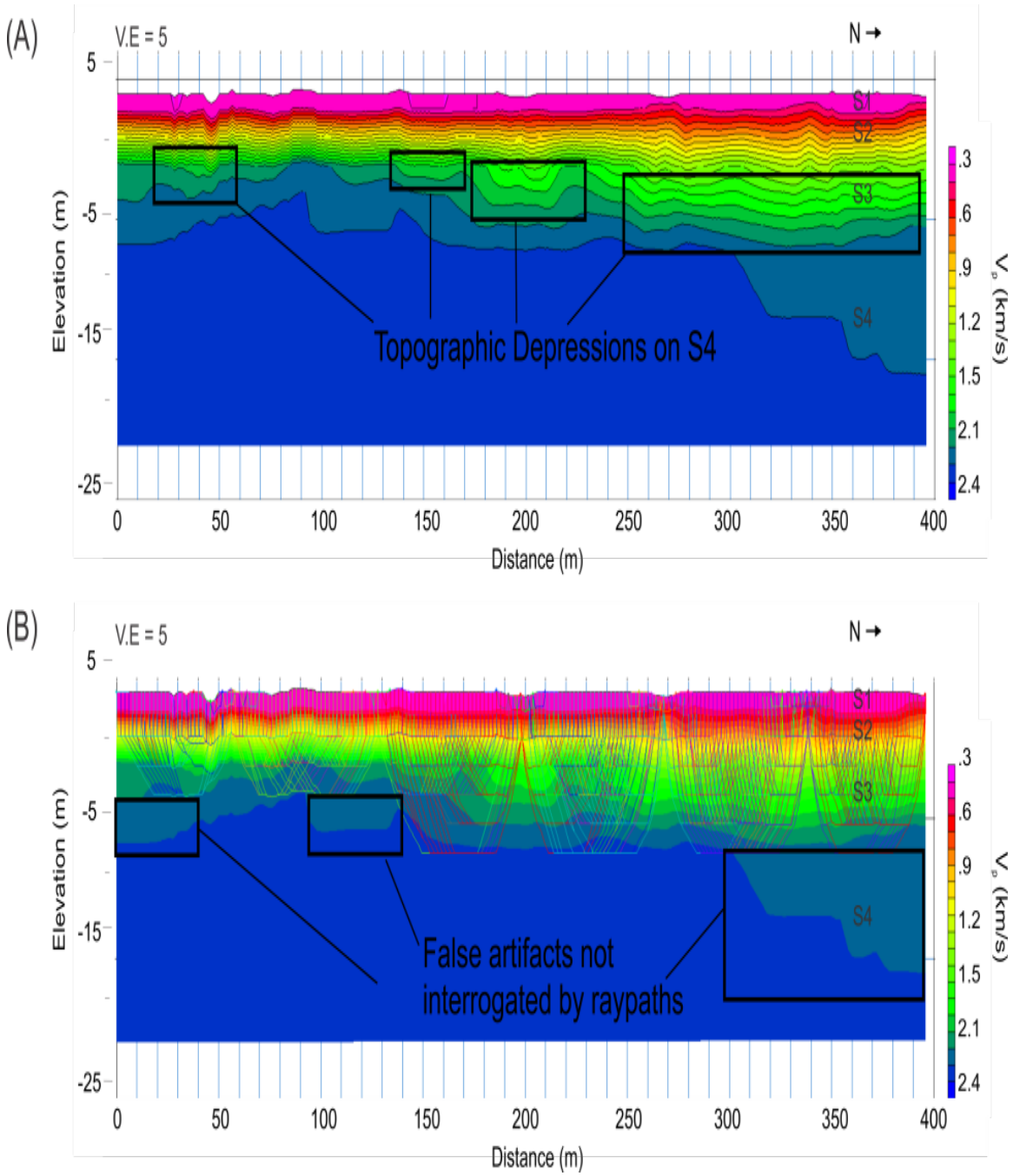

Figure 15. Tomography profiles for Line 1. Layers are denoted on the profiles. Profile A highlights areas of topographic depression on S4. Profile B highlights deep 2.2-2.4 km/s features in layer S4 not interrogated by the modeled seismic raypaths and are not considered real.

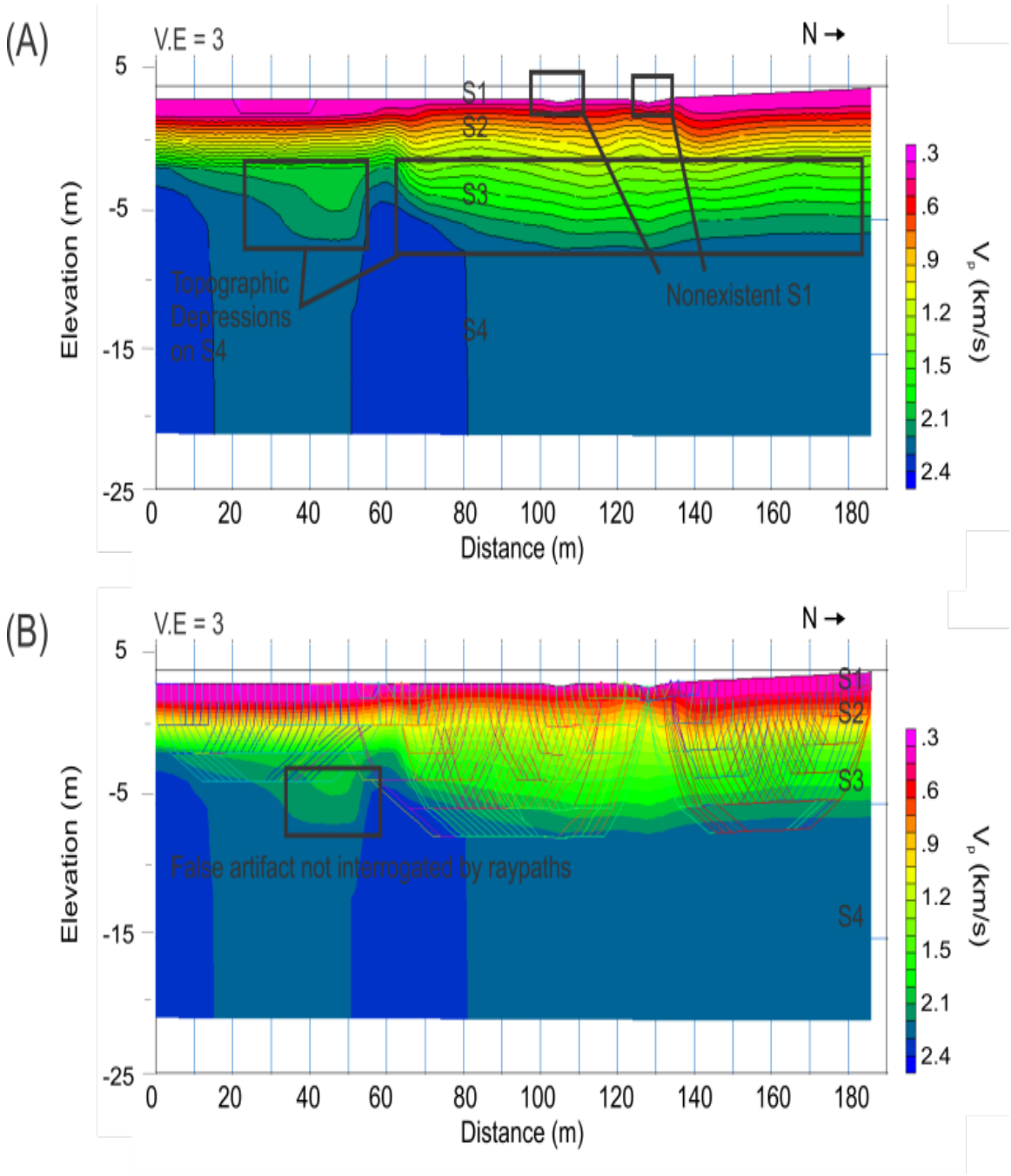

Figure 16. Tomography profiles for Line 3. Layers are denoted on the profiles. Profile A highlights areas where S1 is nonexistent and topographic depressions on S4. Profile B identifies a 1.5- 2 km/s feature on the south side of the profile that is not interrogated by the modeled seismic raypaths, and is not considered real.

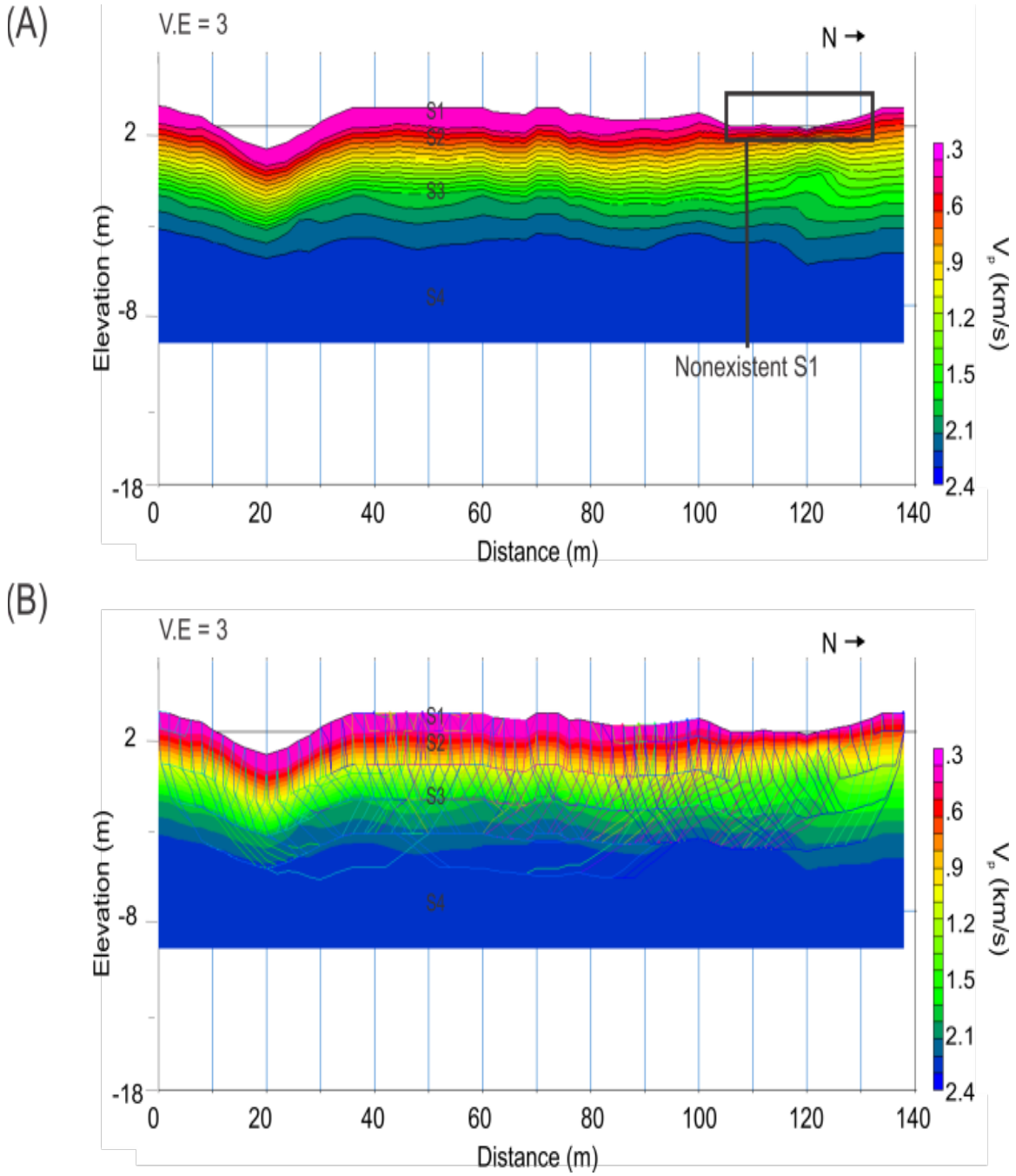

Figure 17. Tomography profiles for UP 2. Layers are denoted on the profiles Profile A highlights an area of nonexistent S1.Profile B shows the profile is thoroughly interrogated.

GPR Results

The GPR profiles within the grid show four radar facies (Figure 18). The first radar facies (RF1) is a thin, continuous, strong reflector seen throughout the GPR grid. The second radar facies (RF2) is dominated by strong, semi-continuous, sub-parallel reflections. RF2 is around 3 – 4 m thick on all profiles (based on the 0.1 m/ns velocity discussed previously and the observed 30 – 40 ns two-way travel time [TWTT] thickness). The third radar facies (RF3) is characterized by a highly attenuated GPR signal that begins at the base of RF2. RF3 extends to the bottom of the profiles at 8.5 m depth (85 ns TWTT). The fourth radar facies (RF4) is characterized by numerous diffractions over areas that are typically 4 meters wide and bounded laterally by RF3. RF4 usually begins at the base of RF2 and persists (mostly as multiples) to the bottom of the profiles at 8.5 m depth (85 ns TWTT). The areal extent of RF4 (Figure 19) reveals two linear semi-orthogonal features that converge at the eastern edge of the map (4 m north and 11.25 m east on the grid). One of the features extends the length of the southern edge of the grid, parallel to the modern stream channel. The other feature runs perpendicular to the modern channel centered around 11.25 m east on the grid. The features connect around 4 m north and 11.25 m east.

Radar facies RF2 is bounded by laterally continuous horizons Hp (pink reflection, at the top of the facies) and Hy (yellow reflection, at the bottom of the facies) (Figure 20). Hp is found at depths of 0.5 – 1 m (5 – 10 ns TWTT) and Hy is found at depths of 3.5 – 4 m (35 – 40 ns TWTT). Within RF2 exist sub-parallel horizontal horizons with a sigmoidal shape, progradationally toplapping each other. These include Hbr (brown), Hr (red), and Ho (orange) (Figure 21). Hbr, Hr, and Ho toplap each other in a prograding pattern at depths of 2 – 3 m (20 – 30 ns TWTT) (Figures 21-22). These horizons downlap onto the base of a laterally continuous

horizon, Hb (blue), near the base of RF2 (Figures 21-22). Hb is found at depths of 2.2 – 3.2 m (22 – 32 ns TWTT) (Figure 21).

Depth below ground surface maps (depth maps), were created for the intervals between Hb, Hbr, Hr, and Ho and the ground surface. The Hb depth map (Figure 23) reveals Hb covering the entire areal extent of the imaged grid. There are bumpy features throughout the horizon, the most prominent being at 8 m north and 7.5 m east (all positions are measured relative to the southwest corner of the grid). In the southern region of the areal extent of Hb exist two elongated features, one relatively deep and one relatively shallow. Another shallow elongated feature exists at 6 m north and 7.5 m east. The Hbr depth map (Figure 24) reveals that the Hbr horizon is limited to the northeast corner of the grid. It terminates by downlapping onto Hb in a southeast trending line starting at 10 m north and 8 m east. The Hr depth map (Figure 25) shows Hr is limited to the northwest corner of the grid. Hr shows bumpy features similar to Hb at 8 m north and 3.75 m and 7.5 m east. The southern extent of Hr, at 4 m north, terminates via downlap along an east trending line onto Hb. The eastern extent of Hr toplaps onto Hbr in a south-southeast trending line starting at 10 m north and 8 m east. The Ho depth map (Figure 26) shows Ho limited to the southern region of the grid. Once again, bumpy features are present in Ho as well as two shallow elongated features from 3 m – 10 m east along 4 m north and from 3.75 m – 11 m along 0 m north. Ho toplaps onto Hr and Hbr along an east–southeast trending line starting at 5.5 m north and 0 m east.

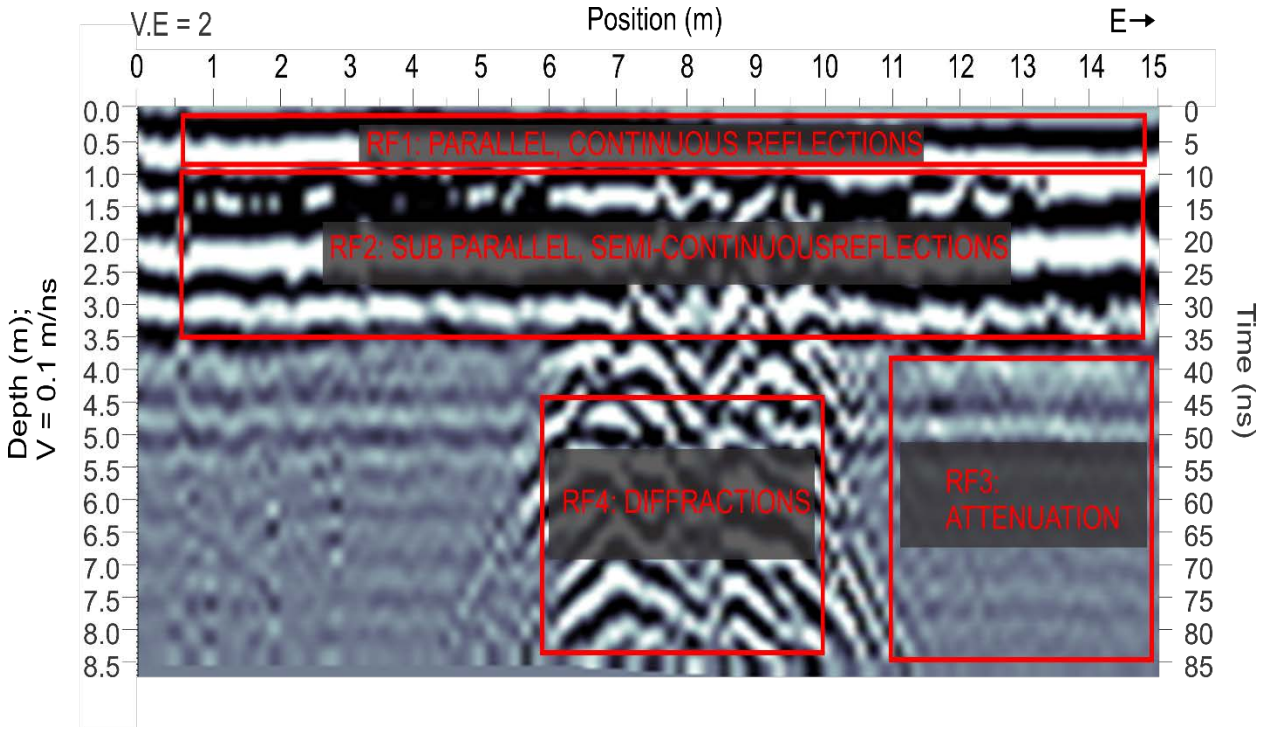

Figure 1814. GL 7, an example of an E-W GL with the four facies highlighted.

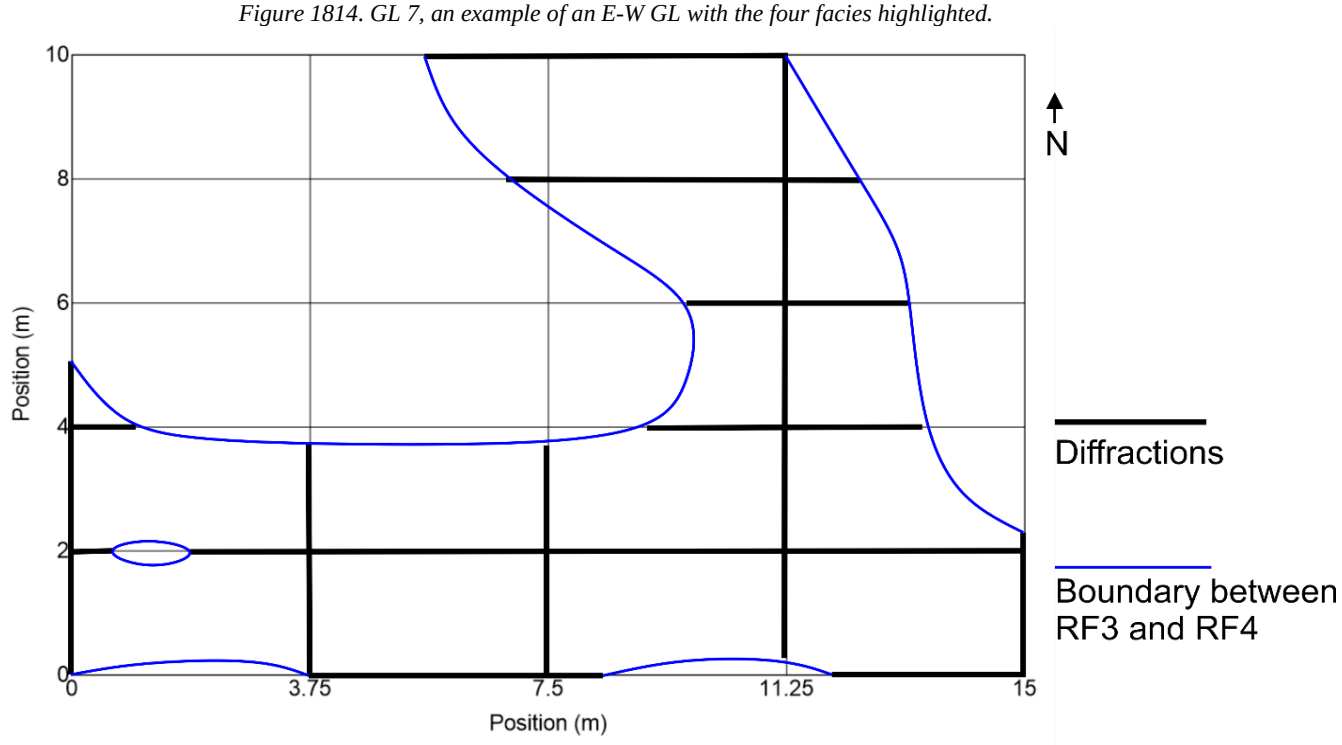

Figure 19. Map view of RF4 distribution. RF4 has a channelized planform.

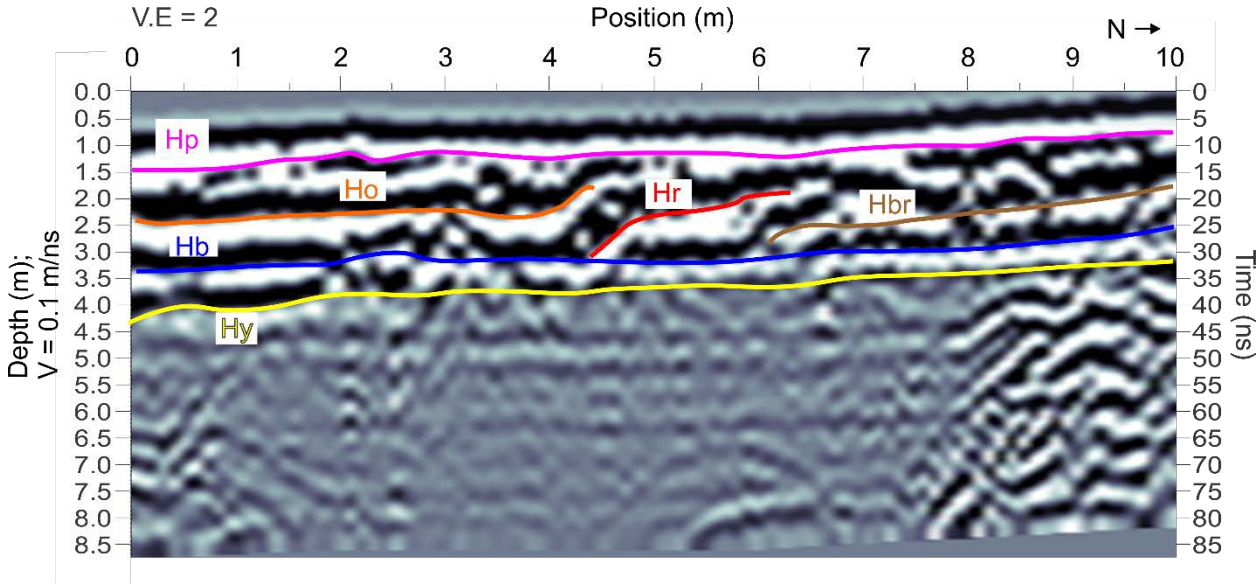

Figure 20. GL 11 with 6 interpreted horizons. Hp and Hy represent facies boundaries while Hb, Hbr, Hr, and Ho represent sigmoidal shaped reflections with progradational toplap ping patterns that downlap onto Hb.

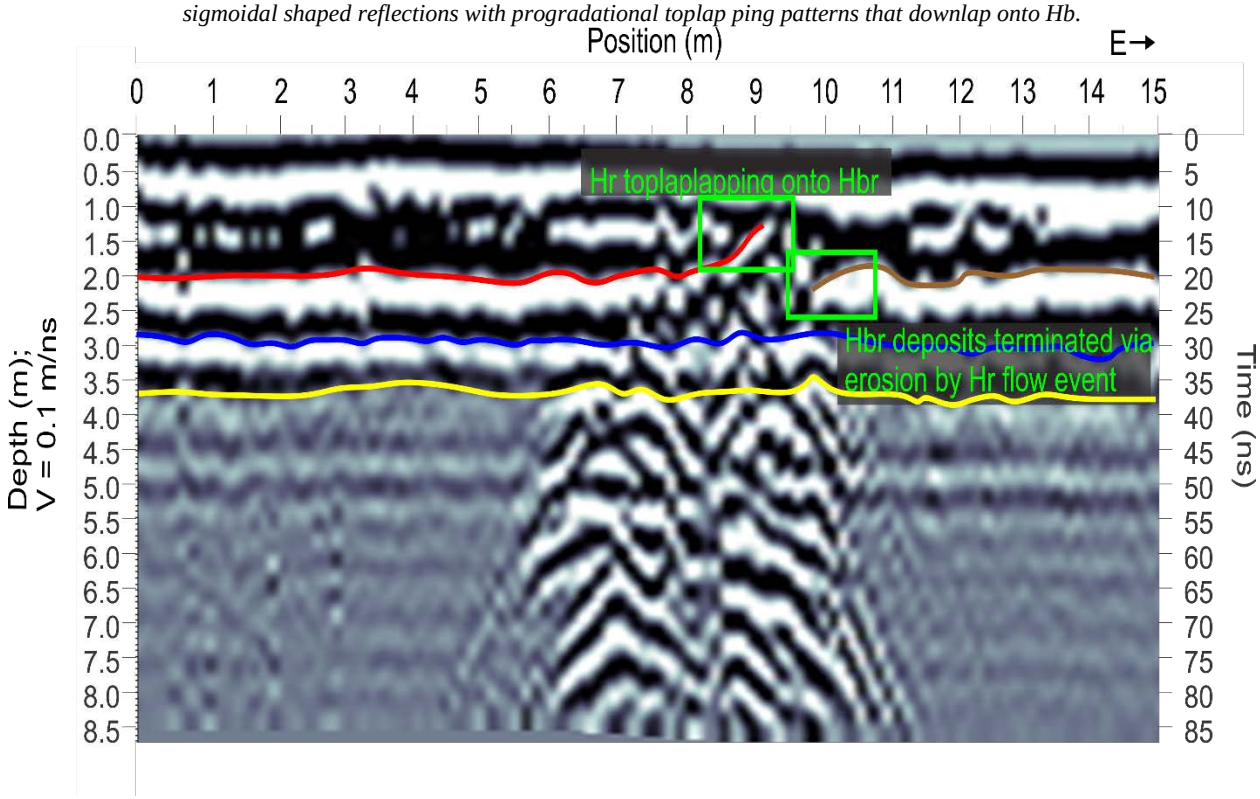

Figure 21. GL 7 with Hy, Hb, Hbr, and Hr traced. Areas of toplap and downlap are highlighted.

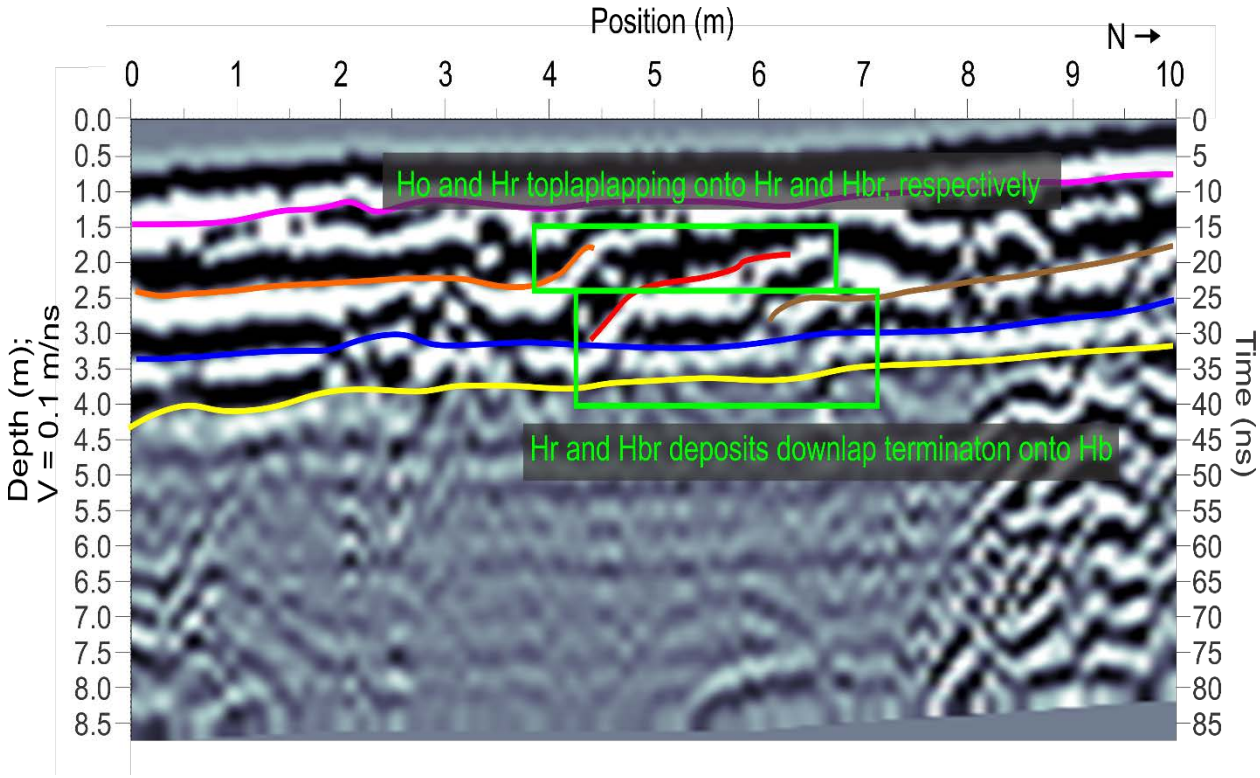

Figure 22. GL 11 with Hy, Hb, Hbr, Hr, and Ho traced. Areas of toplap and downlap are highlighted.

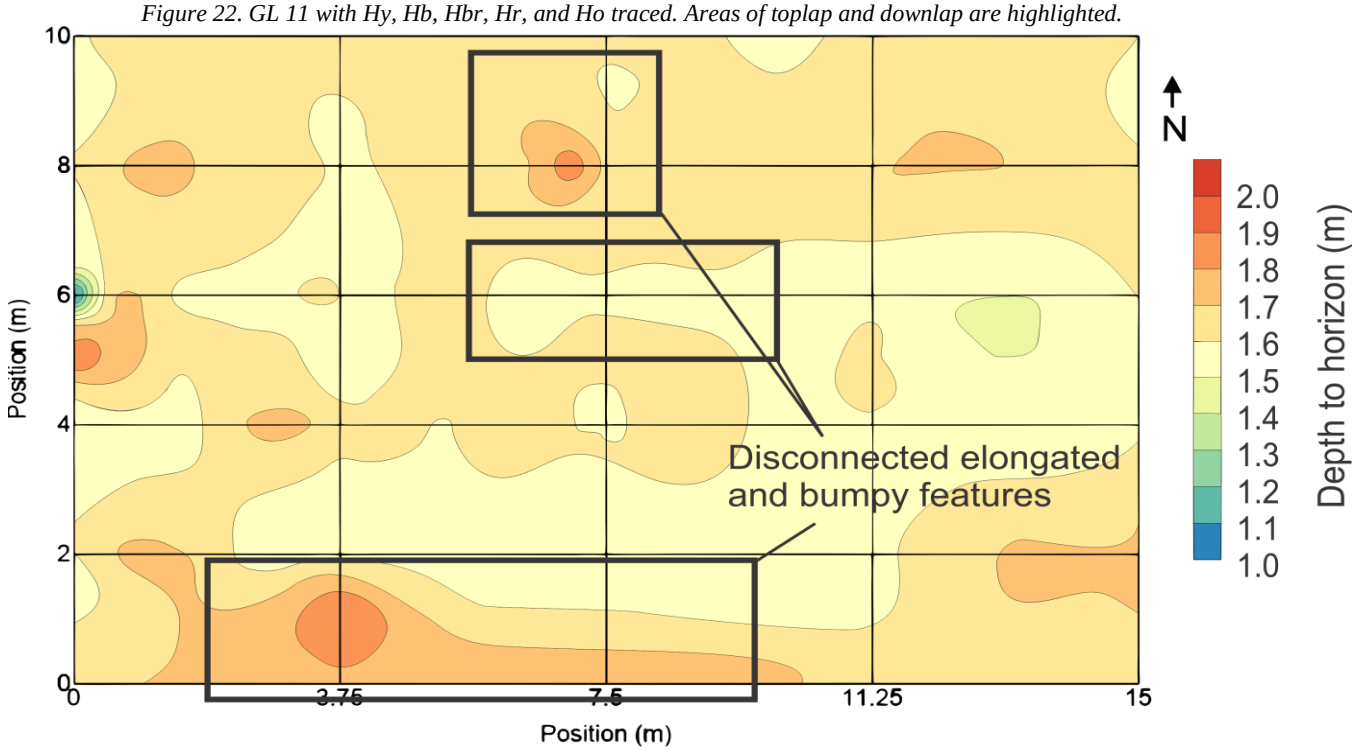

Figure 23. Depth map of Hb. Bumpy and elongated features are highlighted.

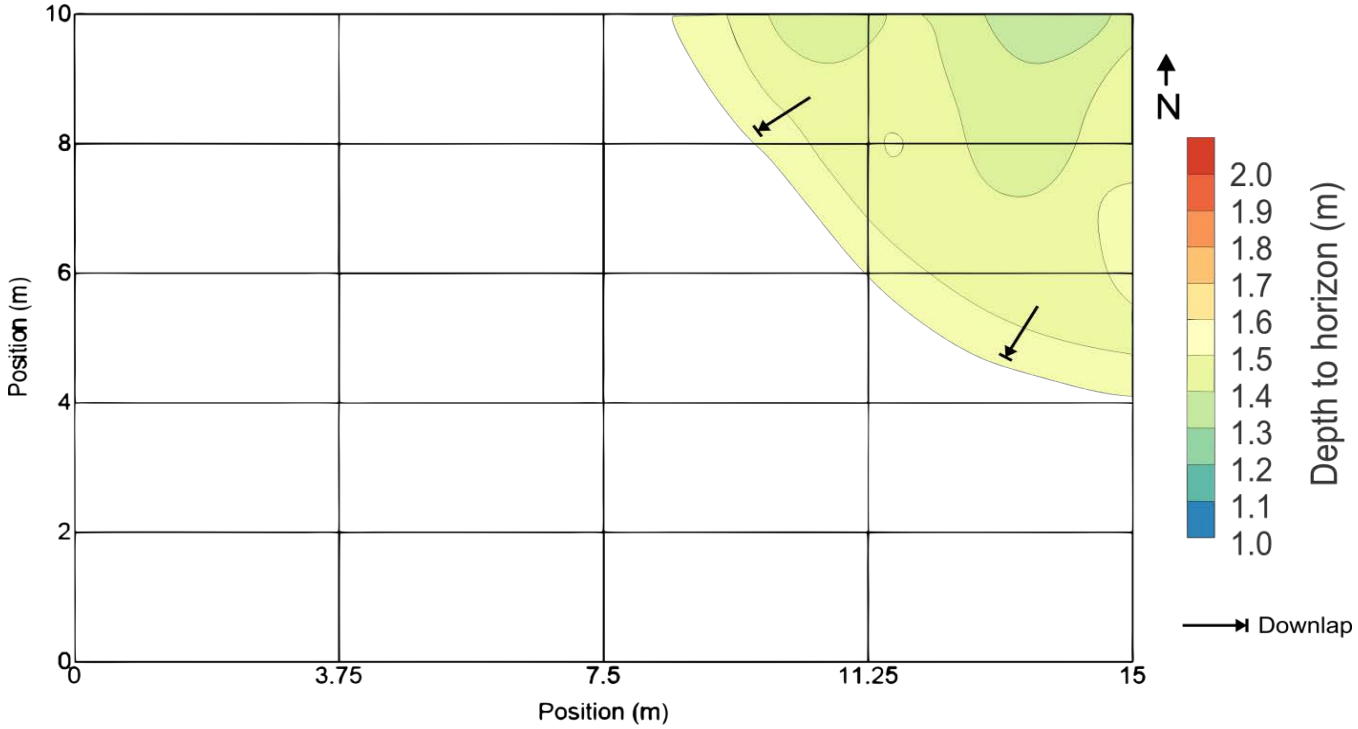

Figure 2154. Depth map of Hbr. Downlap symbols are placed where downlap was observed in the GPR GL.

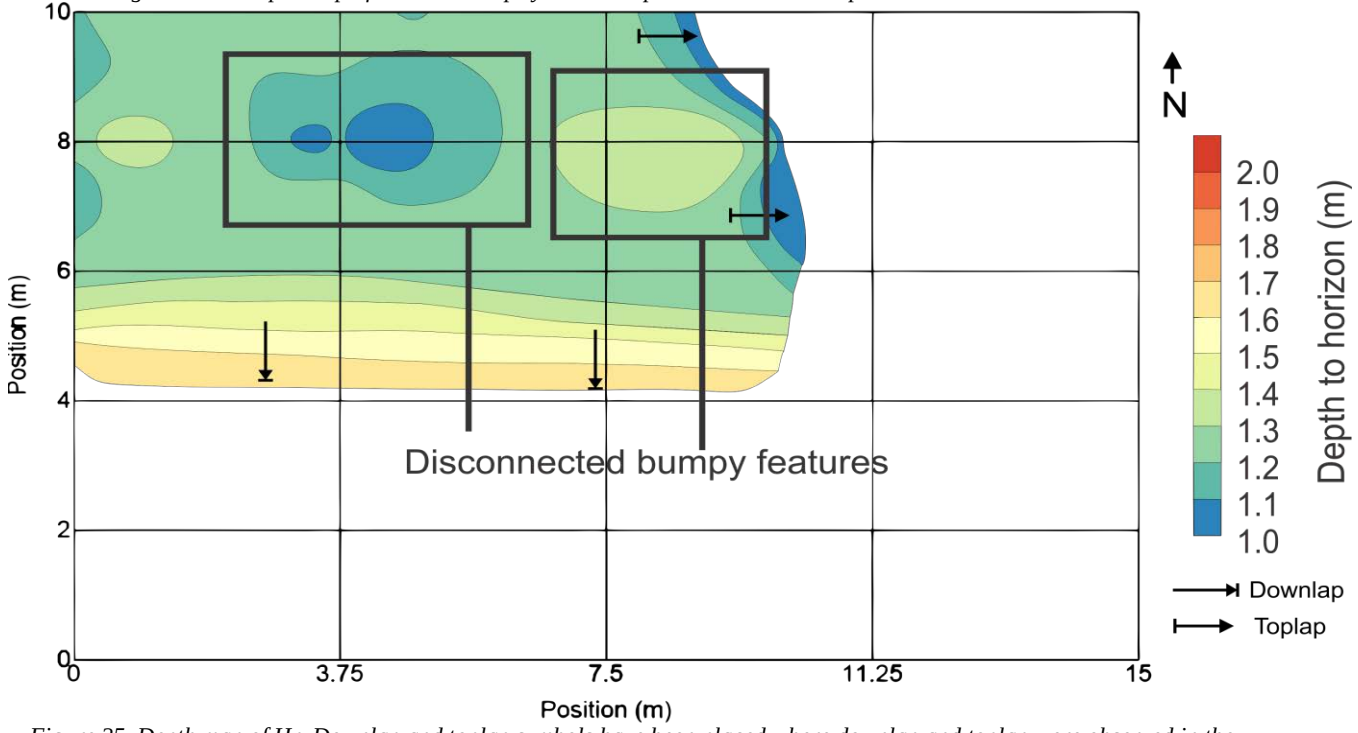

Figure 25. Depth map of Hr. Downlap and toplap symbols have been placed where downlap and toplap were observed in the GPR GL. Bumpy features are highlighted.

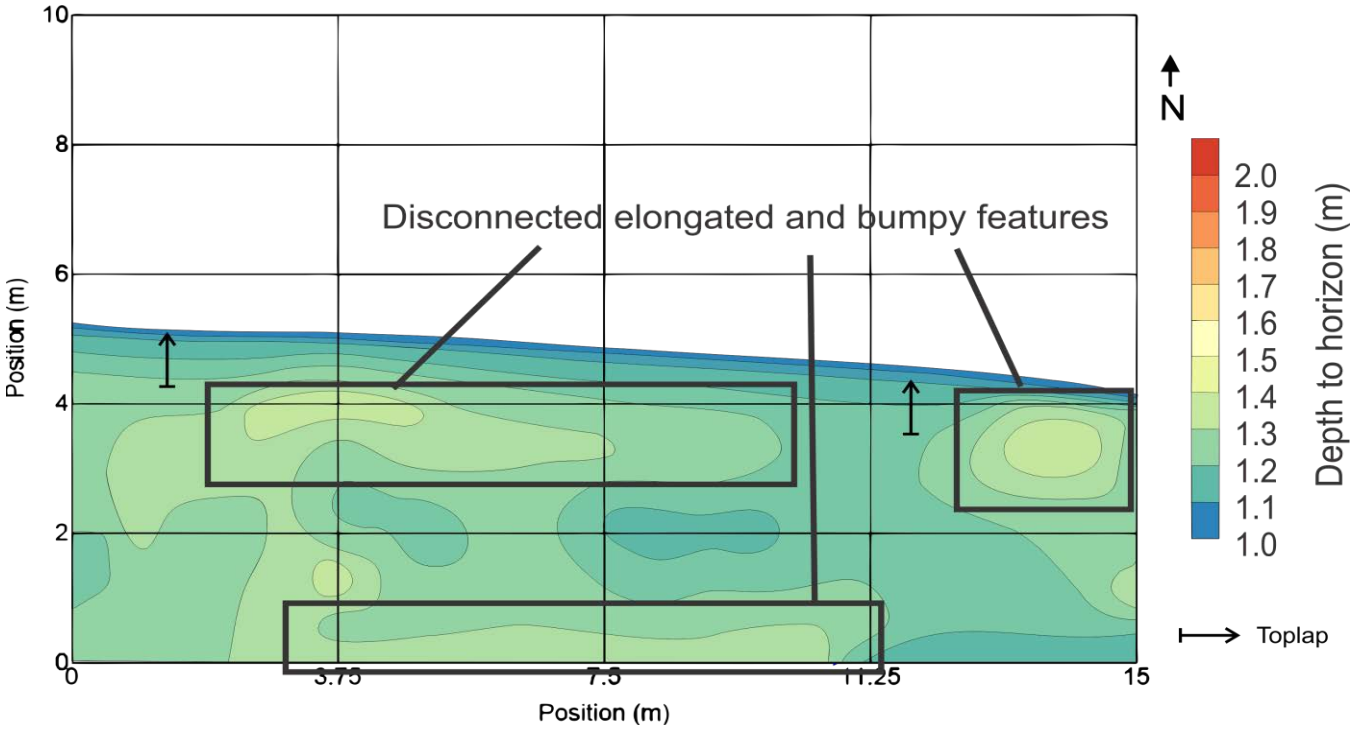

Figure 26. Depth map of Ho. Toplap symbols have been placed where toplap was observed in the GPR GL. Elongated and bumpy features are highlighted.

Interpretation

Seismic refraction layer S4 is interpreted to be the Pierre Shale Formation (Figure 27). The Pierre is known to be the bedrock in the region (Coffin and Horr, 1967) and the seismic velocities (p-wave velocity of 2.3 km/s) are appropriate for shale (Mavko, 2005). In addition, the seismic velocities for the gradational layers, S3 and S2, correspond with alluvium, which is in alignment with the USGS report results (Coffin and Horr, 1967). The nature of the alluvial fill will be discussed further in this section. S1 is interpreted to be eolian sand in agreement with seismic p-wave velocities for dry sand and with field observations of the surface deposits. It is inferred that the most recent floods have scoured away the eolian cap in some places (Figure 28).

The topographic relief on S4 is interpreted to result from incision caused by fluvial activity (Figure 29). The incised areas are usually 20 m wide and 2- 5 m deep, the exception being a much wider incision (150 m) on the north end of Line 1. Across all of the seismic

refraction lines, there are around a dozen 20 m wide incisions on S4. The incisions have sharp channel boundaries and, due to the size, spatial distribution, and number of the incisions, we infer that, prior to deposition of the unconsolidated valley fill, a perennial braided multi-channel system incised into the top of the Pierre Shale. This interpretation is also confirmed by the GPR line spanning the valley bottom as multiple channel boundaries can be identified (Figure 30). S3 is interpreted to be the perennial channel fill as the velocities (p-wave velocities of 1.2 – 2 km/s) correspond to reasonable velocities for compacted, saturated alluvial deposits of intermixed sand, silts, and gravels. GPR radar facies RF3 and RF4 image the same interval of sediments as S3 and allow for a higher resolution interpretation of the alluvial fill within the perennial channel system atop the Pierre Shale (Figure 31). The diffractions within RF4 are interpreted to be caused by cobbles within lag-deposits that accumulated in places at the bottoms of channels after high-energy flows. It is important to note, that the cobbles are interpreted to have come from localized sources and are not believed to have been transported from the headwaters near the Rocky Mountains as the channel lacks flow power to transport cobble sized materials over that distance. Their areal distribution, mentioned earlier (Figure 19), is interpreted to result from deposition in two intersecting sub-channel branches within the braided multi-channel system. We also infer that the high-energy flows that deposited the coble sized sediments led to overbank flow that deposited clay sized sediments outside of the channel boundaries. RF3 is interpreted to be these deposits, with the highly attenuated signal attributed to the clay-rich material.

A change in the nature of deposits occurs between S3 and S2, and RF3/RF4 and RF2 (Figure 31). S2 has a sharp velocity gradient with p-wave velocities of 0.5 – 1 km/s that correspond to unconsolidated, dry alluvial deposits of intermixed sand, silts, and gravels. This sediment lithology is confirmed by the USGS report that denotes the valley fill as coarsening

downward into sands, silts, and gravels (Coffin and Horr, 1967). The high velocity gradient in S2 is in contrast to the low velocity gradient in S3 and is interpreted to be due to layered changes in sediment composition as well as compaction at the base of S2. Bedding structures within the S2 interval are imaged in GPR facies RF2. The GPR data show a clear contrast in the nature of the reflections from RF3/RF4 to RF2. As opposed to RF3/RF4, there are no clear channel fill/over-bank deposit sequences within RF2, and RF2 does not have any diffractions indicative of cobble sized or larger sediments. RF2 is composed fully of sigmoidal shaped, sub-parallel horizontal horizons (Figure 32). The areal extent of the horizons does not show any channel-like features (incisions or sidelap), but reveals bumpy, disconnected, and elongated features with no clear pattern (Figures 33-36). Due to the lack of well-defined channel boundaries, absence of large cobble sized particles, and bumpy, disconnected, and elongated features, we infer that the deposits imaged in S2 and RF2 are deposited in an ephemeral channel system. An ephemeral channel system does not have sustained flow to create stable channel boundaries, and the lack of consistent flow leads to a lack of flow power sufficient to transport and deposit cobble sized sediments. Ephemeral channels rely on localized, sporadic flows to create surface flow, which leads to disconnected depositional features that appear bumpy and elongated when viewing the areal extent of the deposits. Due to the lack of time constraints, it is possible that RF2 was deposited during one abnormally large flood. However, it is believed to be more likely that RF2 was deposited as a result of multiple floods; hence, the following interpretations assume multiple floods depositing RF2.

The features that are deposited by the ephemeral channel system are only found within the modern channel boundaries, leading to the interpretation that ephemeral channels do not have

sufficient surface flow to migrate episodically or gradually across the valley bottom. Rather, the ephemeral stream system is stationary within the valley.

However, as mentioned, in places RF2 contains multiple, stacked, sigmoidal shaped, sub-parallel horizons that are interpreted to indicate sub-channel boundaries or bars within the main ephemeral channel (the termination of the channel boundaries is not imaged in the grid profiles but is known to be at the edge of the profile as confirmed by the location of the channel imaged on the GPR line spanning the valley bottom). The sigmoidal reflectors are interpreted to each have been deposited in a distinct flood. Their geometry and stacking patters allow three alternative depositional models: DM1 (lateral accretion of bars or sub-channel boundaries), DM2 (aggrading sub-channel), and DM3 (mixed). The first depositional model, DM1, is a laterally accreting model (Figure 37). In DM1, Hb is the oldest horizon that blankets the imaged area (Figure 33). Hbr is deposited in a subsequent flow, blanketing Hb (Figure 34) from the north, as interpreted from the mapped distribution of the downlap directions. A third flood, flowing in a more southeasterly direction, erodes almost all of Hbr except for a small region in the northeast of the grid. The third flood deposits a new horizon, Hr (Figure 35). A similar process occurs for Ho, with a flood first eroding all of Hr except for a small region in the northwest of the imaged area, and then depositing the east-trending Ho (Figure 36). Most recently, floods have become too sporadic to blanket the region in sediment or cause sub channels to form, and the region has been covered in an eolian cap, Hp. Model DM1 assumes enough power for each flow to erode previous deposits on the bar or sub-channel banks. Depositional model DM2 interprets the horizons as an aggrading sequence. In DM2 (Figure 38), Hb is the first flow that blankets the region. Subsequently, the Hbr flow deposits another blanketing horizon with a sub channel boundary at 6 m north on GL 11. A third flow deposits another blanket of sediment, Hr, on top of

Hbr, with a sub channel boundary at approximately 4.3 m north on GL 11. The third flood deposits the last blanket of alluvial sediment, Ho, on to the region. The sub channel boundary for Ho is at 4 m north on GL 11. As in DM1, recent flows have become too sporadic to blanket the region in sediment or cause sub channels to form, and the region has been covered in an eolian cap, Hp. Model DM2 assumes each flow has sufficient sediment supply to cause aggradation, while not enough power to erode deposits from previous flows. Lastly, depositional model DM3 is both aggradational and laterally accreting. For DM3 (Figure 39), Hb extends to 6 m north on GL 11 where it is terminated by Hbr. Hbr blankets the north end of GL 11 and creates a sub channel boundary at 6 m north on GL 11. At approximately 4.75 m north on GL 11, Hbr is eroded by the Hr flow. The Hr flow creates a sub channel with boundaries at 6.5 m north on GL 11 and blankets the southern portion of GL 11. Lastly, Ho is deposited on top of Hr in an aggradational flow. As in the other models, recent flows have become too sporadic to blanket the region in sediment or cause sub channels to form, and the region has been covered in an eolian cap, Hp. Model DM3 assumes that each flow has variation in flow power and sediment supply and can result in erosion of previous flows or aggradation on top of previous flows. All three depositional models are viable, but after correlating all of the horizons on all of the GPR grid lines, I believe that in this case, DM1 is the most reasonable.

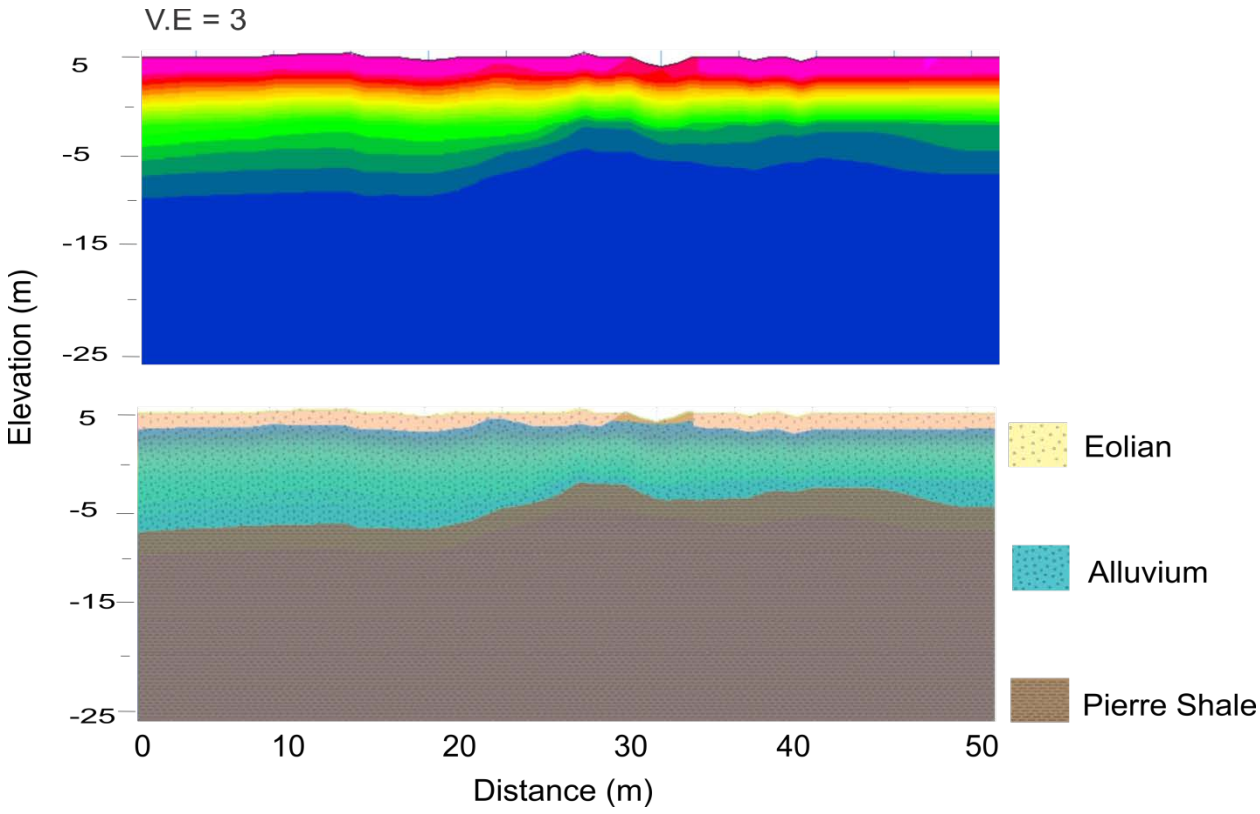

Figure 27. A portion of a Line 2 with the interpreted facies overlaid on the tomography profile. The darkened eolian region is a high velocity anomaly and interpreted to be saturated eolian sands.

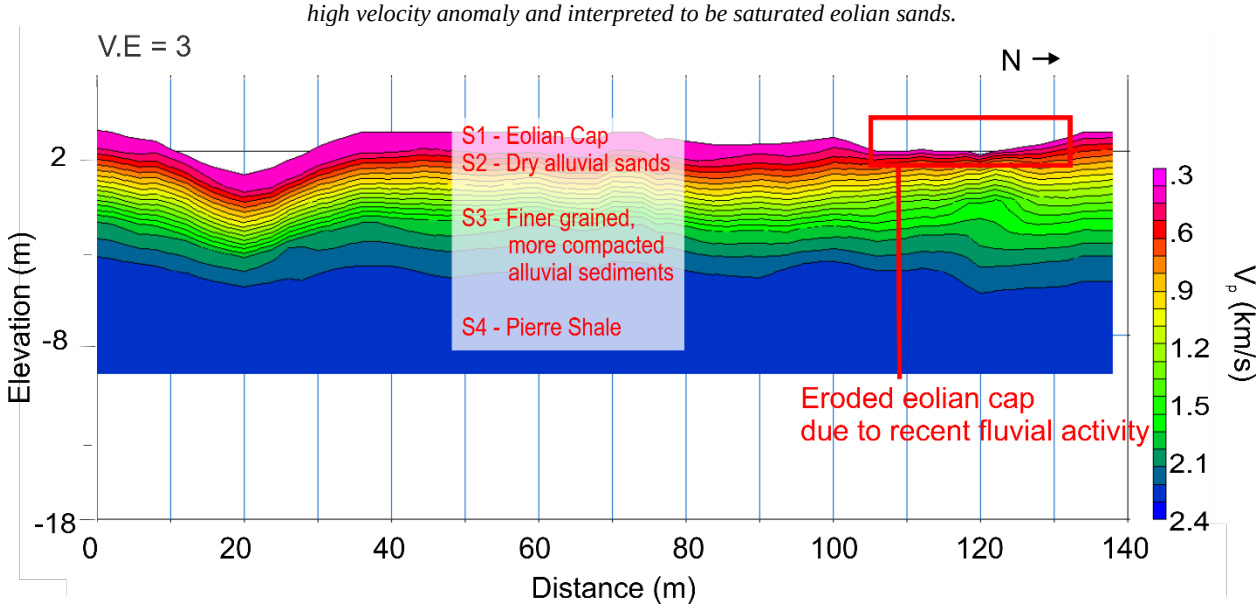

Figure 28. UP2 Tomography profile with the four seismic layer interpretations. The highlighted area of eolian cap erosion is due to modern fluvial activity.

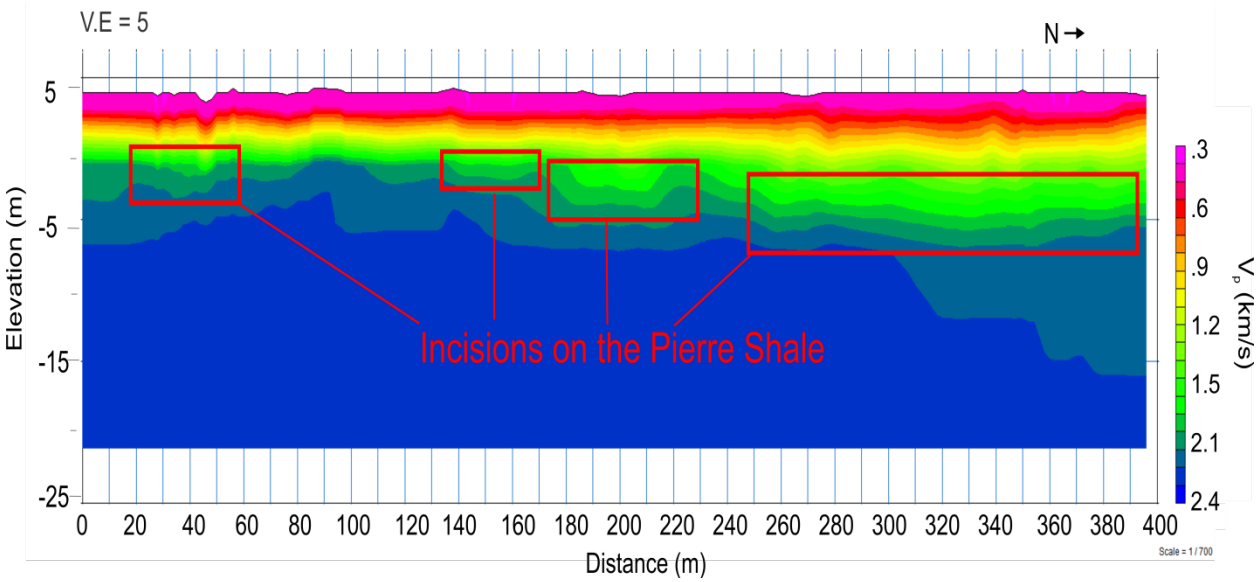

Figure 29. Line 1 tomography profile with identified incisions on the Pierre Shale due to a lowering of base level and fluvial activity with high powered flows.

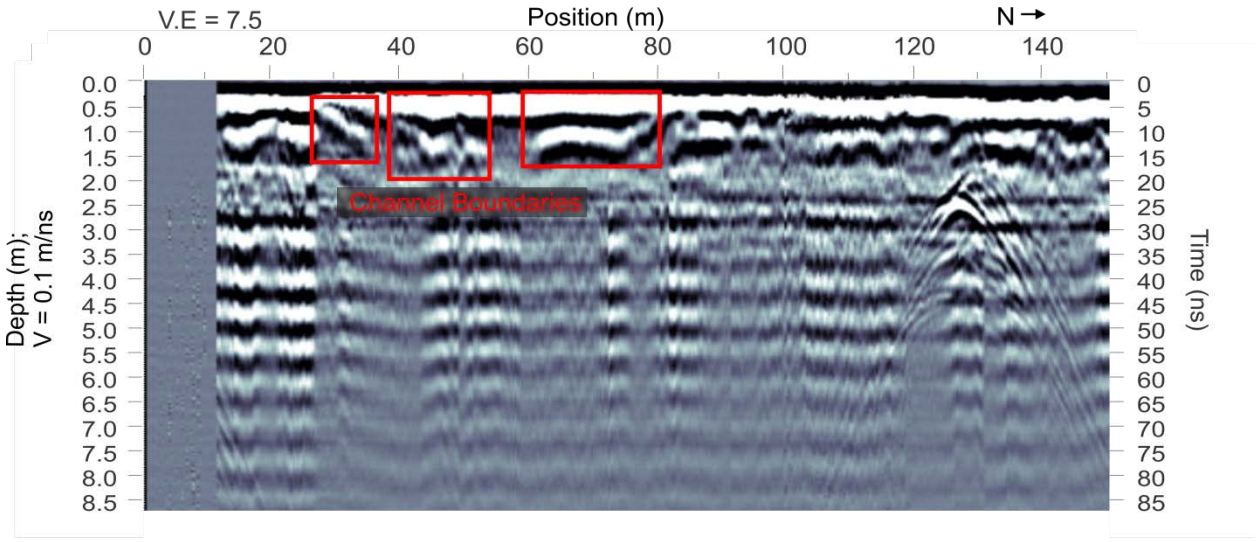

Figure 30. GPR Line 1 confirming channel boundaries interpreted to have been created by a perennial braided channel regime in the past.

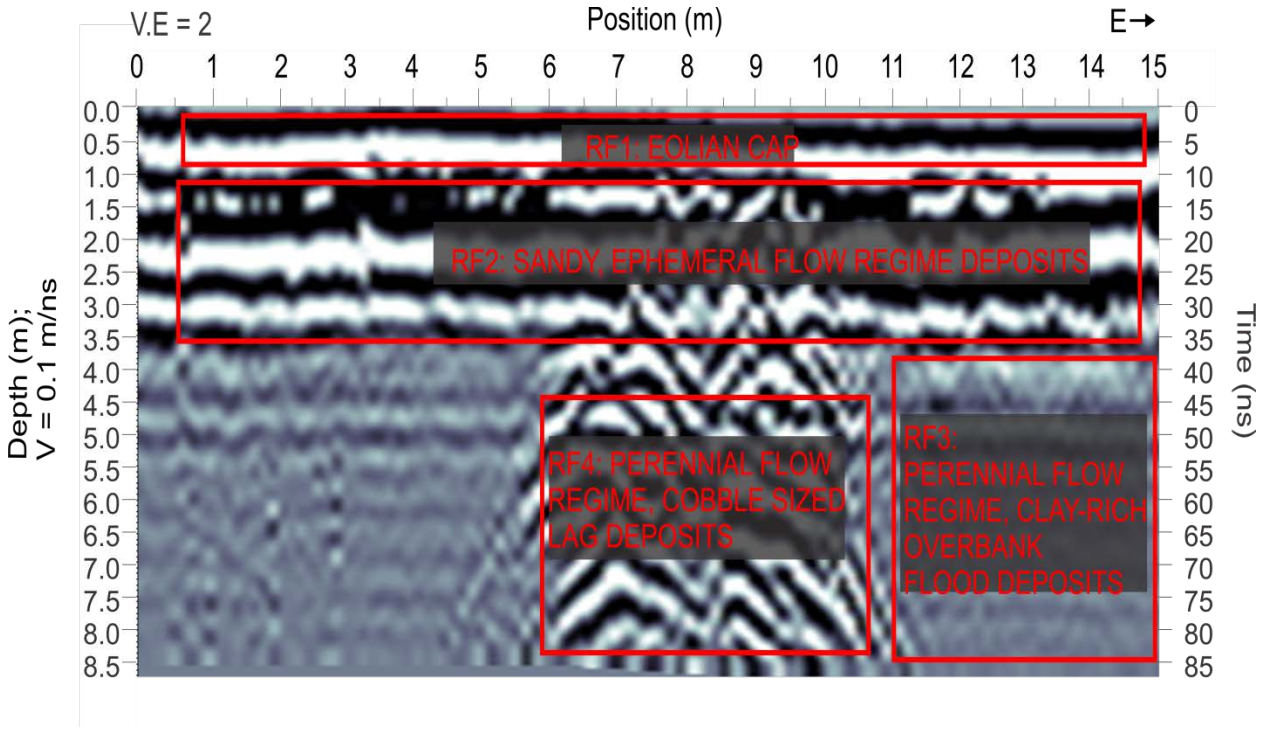

Figure 31. GL 7 with the interpretation of the four radar facies.

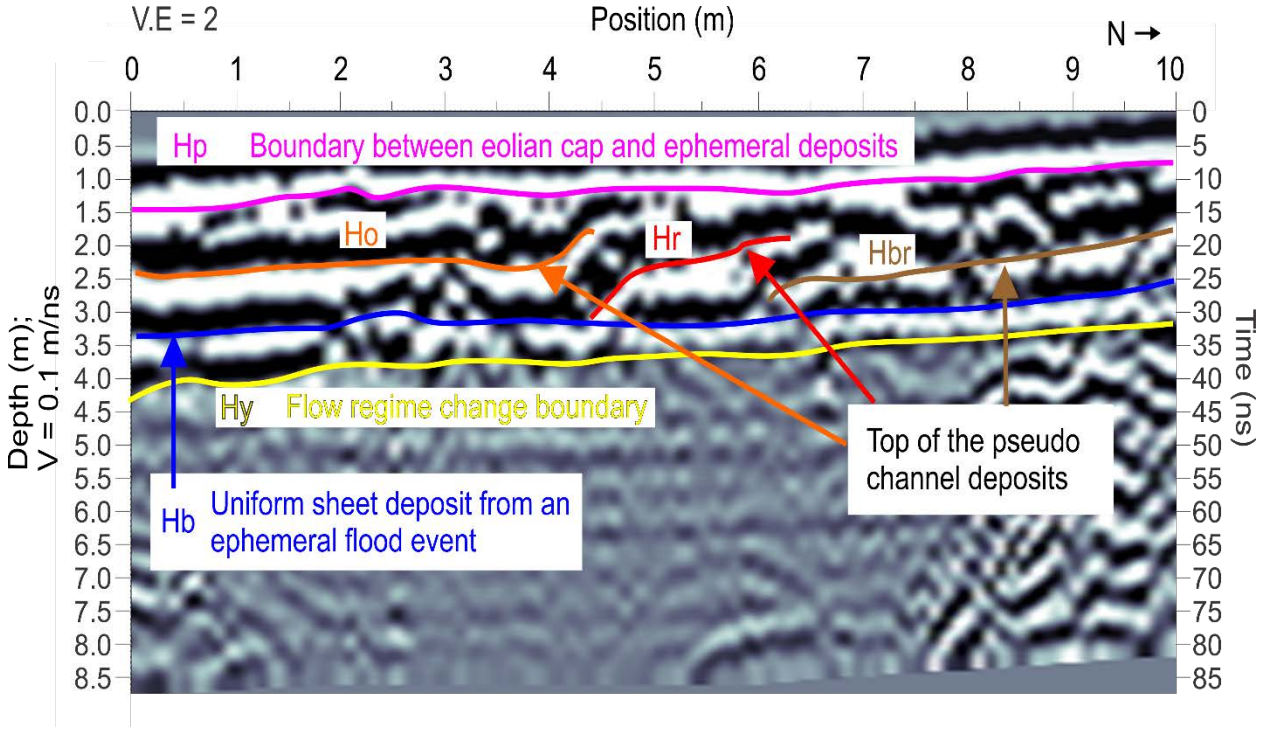

Figure 32. Horizon interpretation for GL 11.

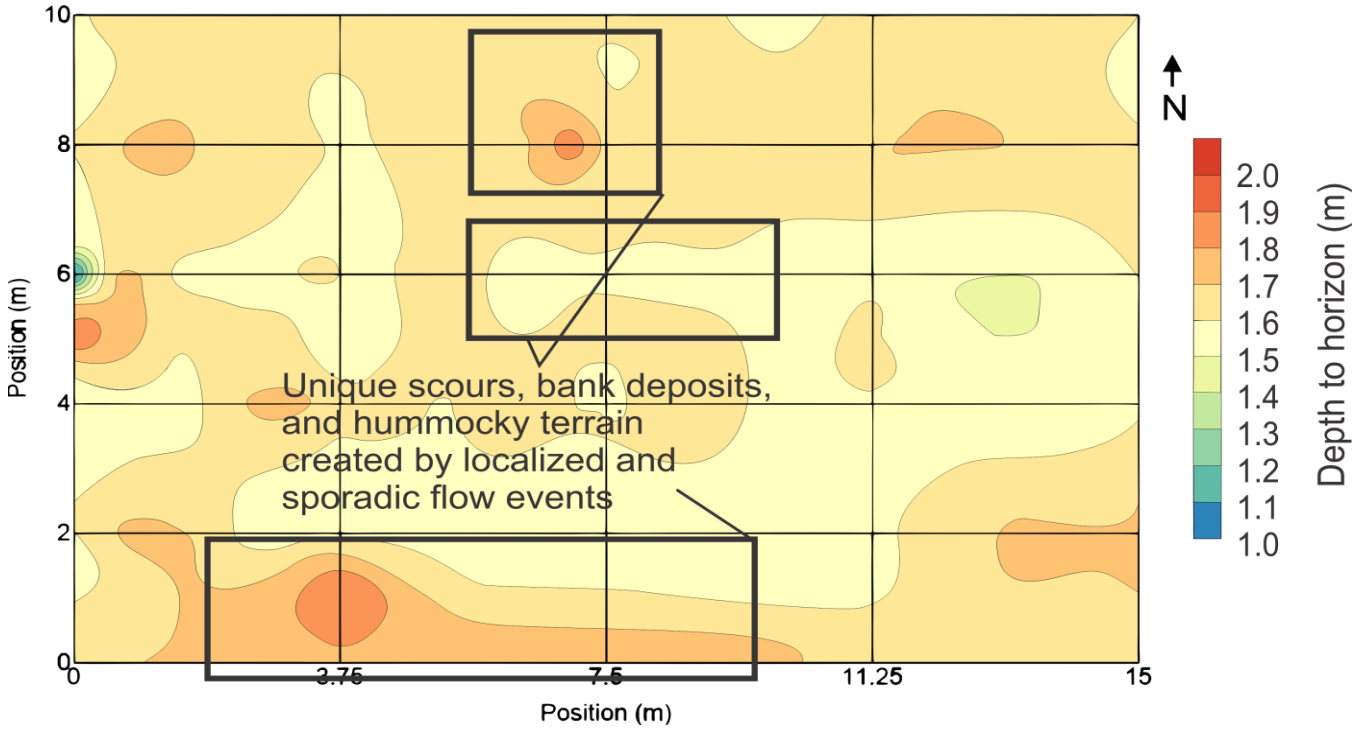

Figure 33. Depth map of Hb. Hummocky topography, banks, and scours created by sporadic localized flow are highlighted.

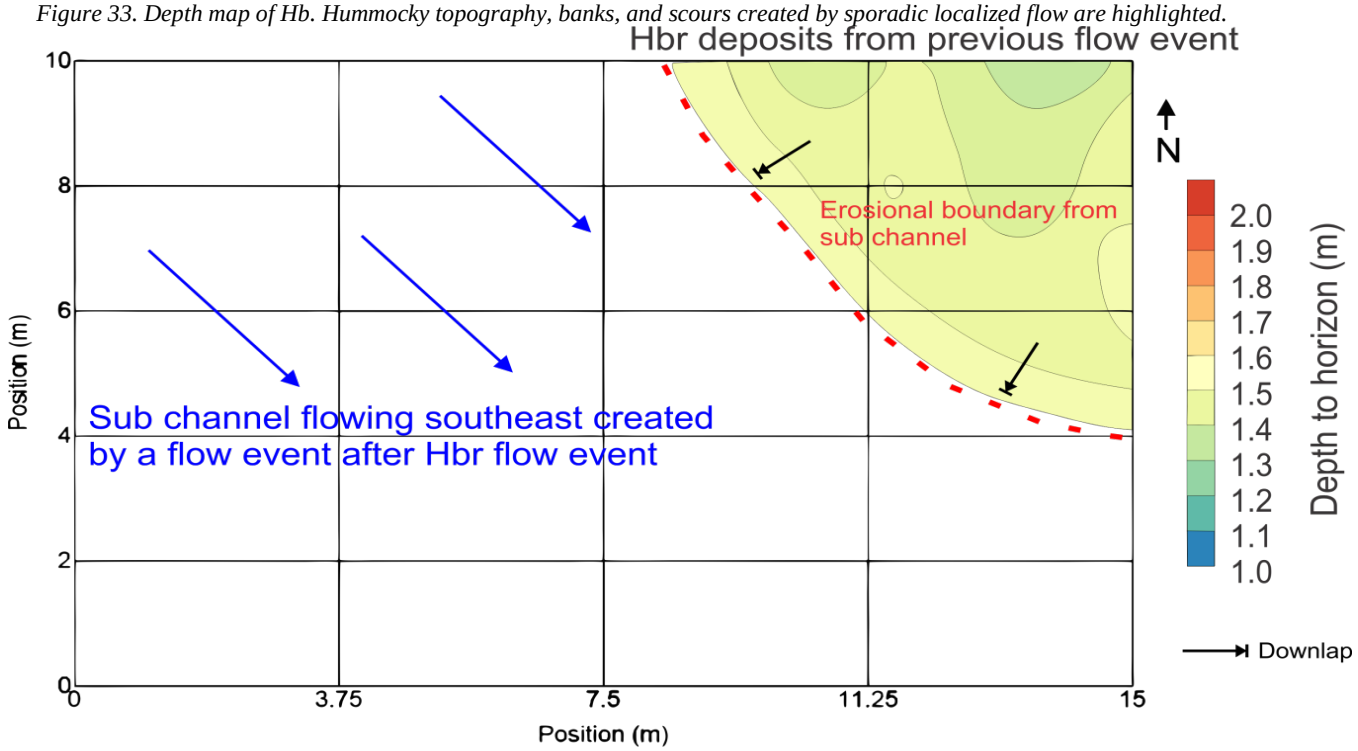

Figure 34. Depth map of Hbr. Hummocky topography, banks, and scours created by sporadic localized flow are highlighted. The erosional boundary from the southeasterly flowing sub channel is traced.

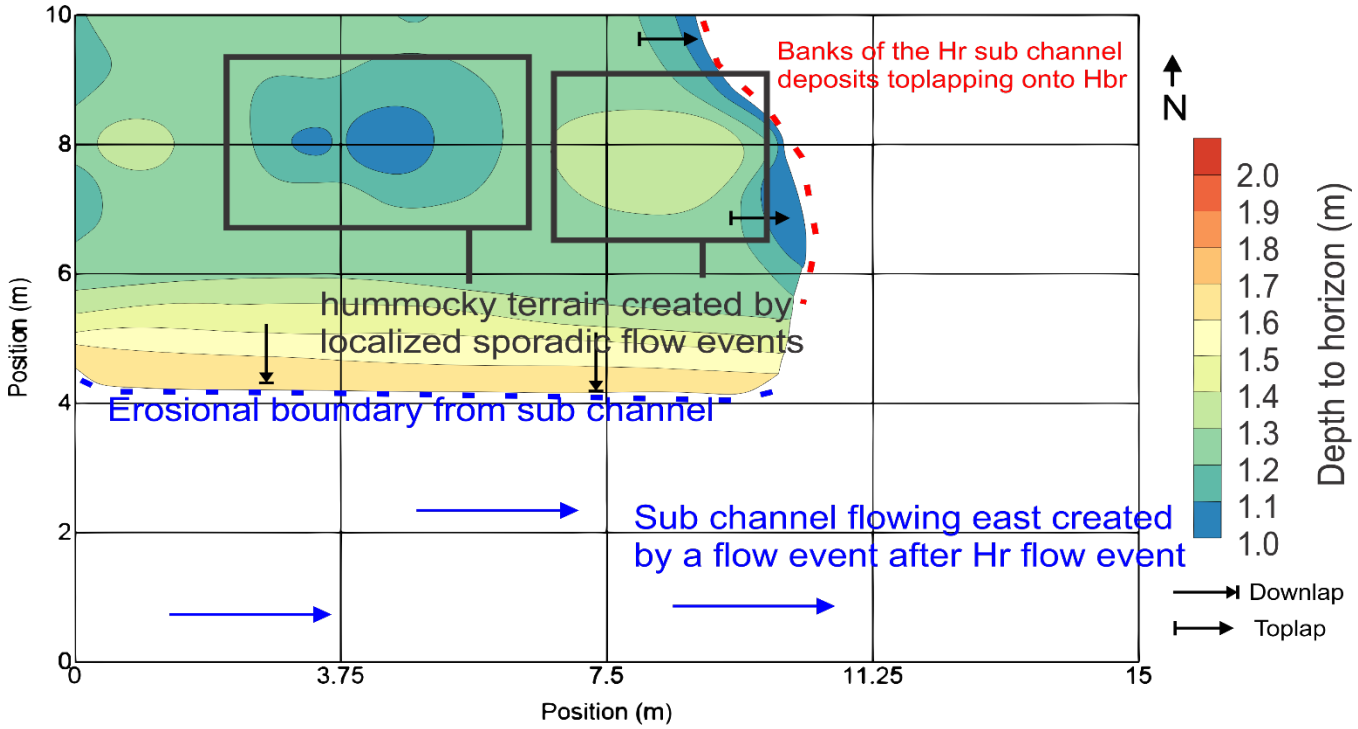

Figure 35. Depth map of Hr. Hummocky topography, banks, and scours created by sporadic localized flow are highlighted. The erosional boundary from the easterly flowing sub channel is traced. Also traced are the Hr deposits toplapping onto Hbr.

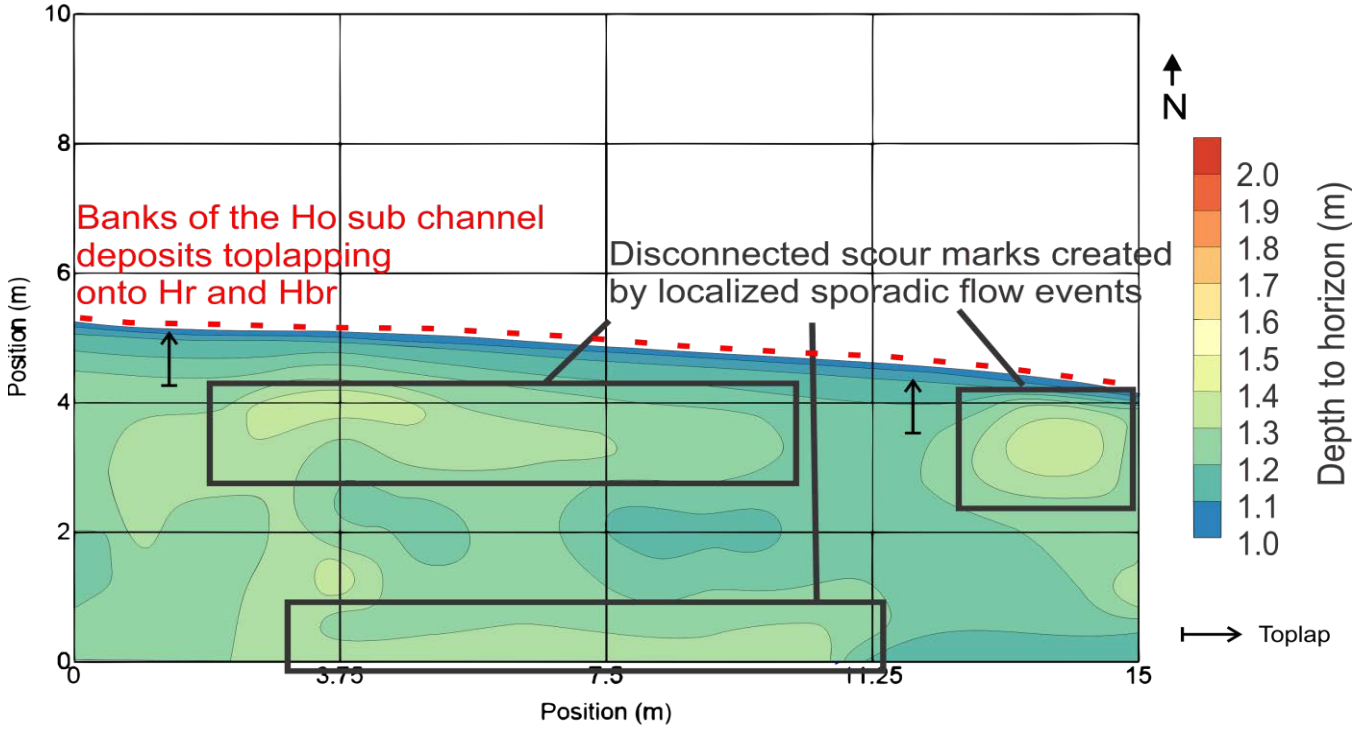

Figure 36. Depth map of Ho. Hummocky topography, banks, and scours created by sporadic localized flow are highlighted. Ho deposits toplapping onto Hr and Hbr are traced.

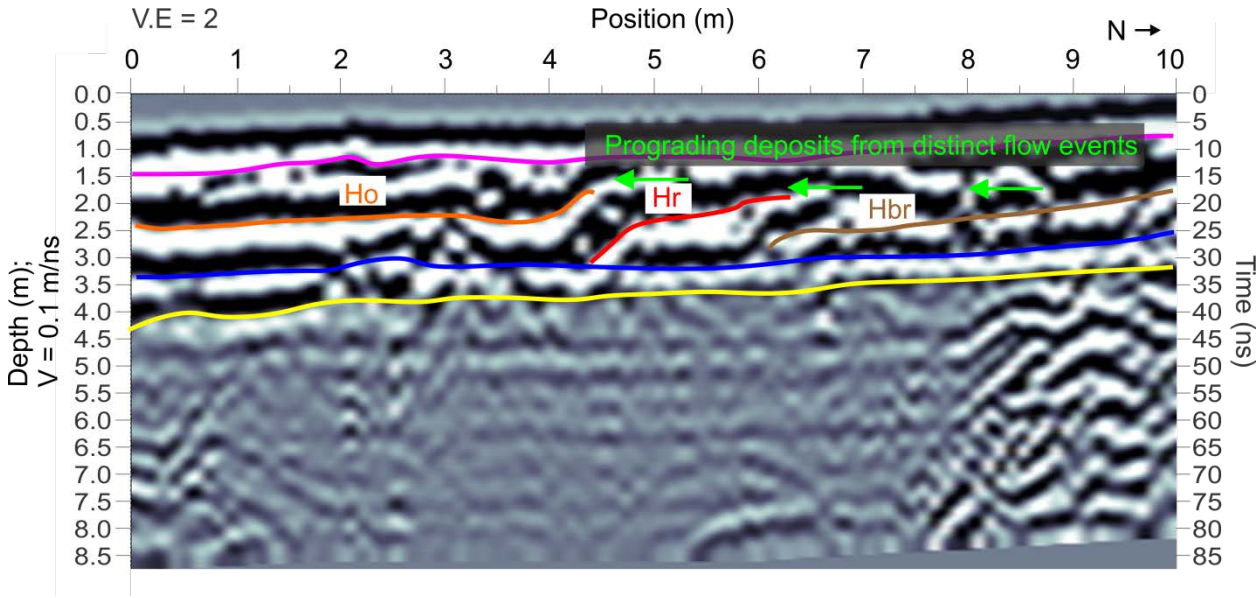

Figure 37. GL 11 showing the laterally accreting model DM1.

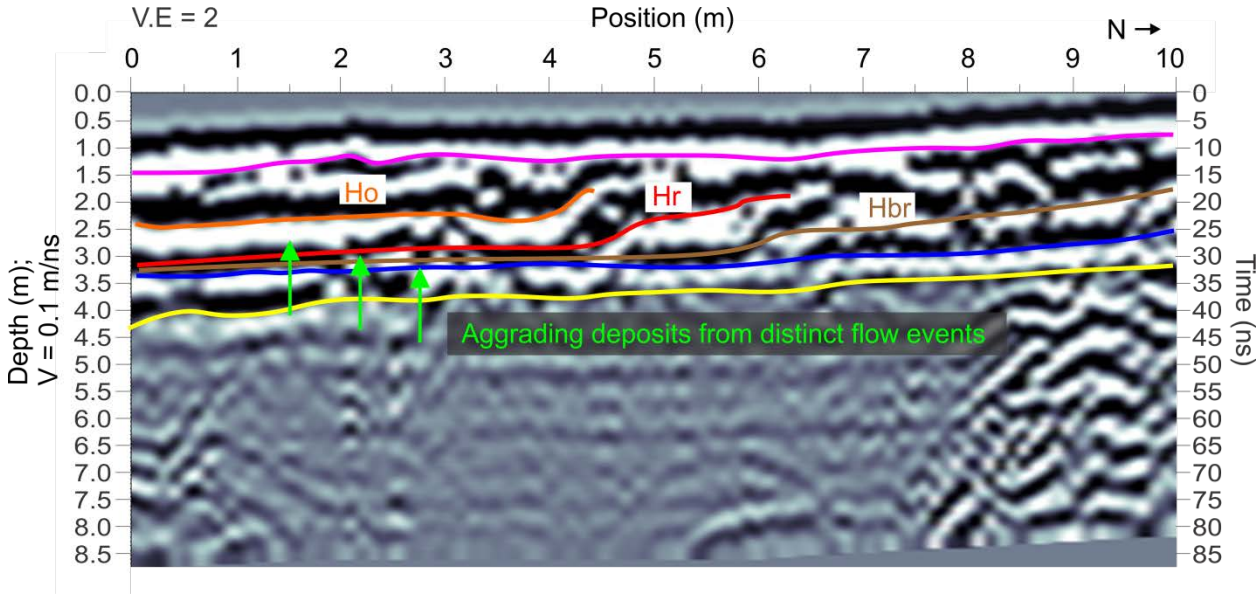

Figure 38. GL 11 showing the aggradational model DM2.

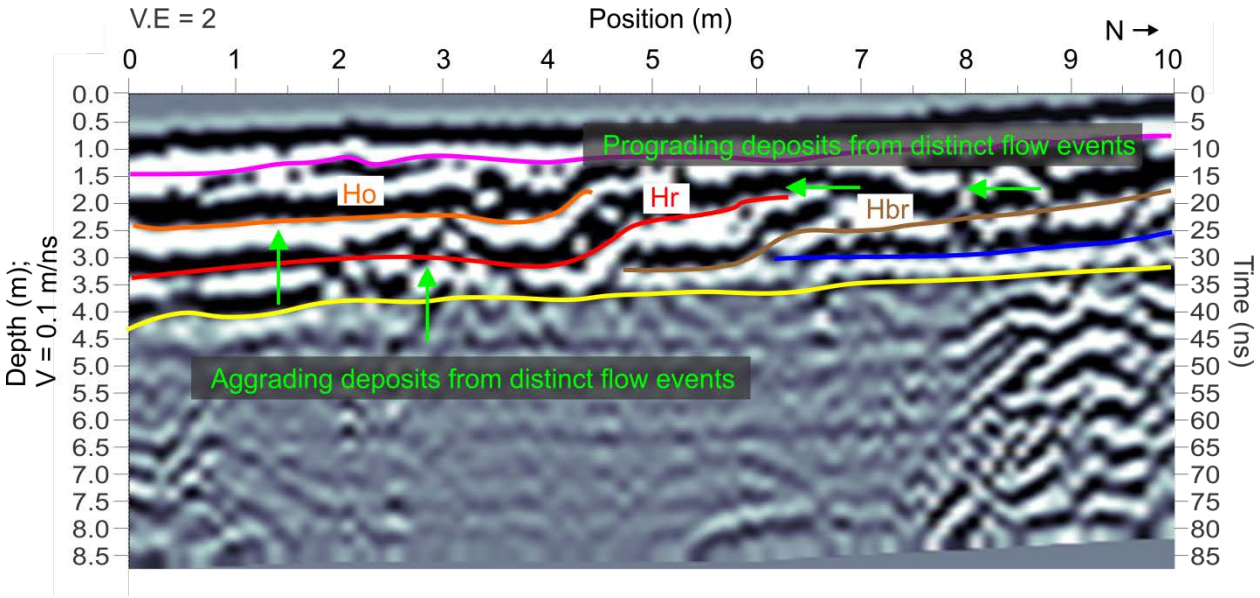

Figure 39. GL 11 showing the aggradational and laterally accreting model DM3.

Interpretation of the Evolution of Sand Creek

The integrated analysis of the refraction and GPR images of the alluvium shows two differing fluvial regimes have dominated at different times at Sand Creek. The oldest non-marine (post-Pierre Shale) strata in the valley were deposited in a perennial braided multi-channel system after a base level fall exposed the Pierre Shale and allowed fluvial incision. The perennial channel system, characterized by consistent flow with occasional high energy flows, scoured multiple channels into the Pierre Shale, as evidenced in all of the seismic lines throughout the valley. The GPR grid survey imaged the deposits within the perennial channel system. The diffractions seen in the bottom half of the GPR grid profiles were caused by cobble sized lag deposits transported by floods. In the same floods, clay-rich overbank flood deposits were deposited in the regions bounding the cobble filled scours. The mapped cobble filled scours reveal two converging stable paleo-channels, bolstering the interpretation of a perennial channel system with multiple channels flowing throughout the valley.

At some point, a flow regime change occurred at Sand Creek. The p-wave velocity changes between S2 and S3 in the seismic lines and deposition of horizon Hy in the GPR grid (both at a depth of around 4 m) represent the flow regime change. The Sand Creek drainage transitioned from a perennial channel system to an ephemeral channel system. The ephemeral channel system is characterized by a lack of well-defined channel boundaries, a lack of sediment larger than gravel, and areally disconnected features that are bumpy and elongated due to localized, sporadic flow. The three alternative depositional models for the ephemeral stream deposits all recognize multiple floods/depositional events that form laterally accreting and/or aggrading bars and/or sub channels within the larger ephemeral stream system. However, all of these depositional events occur within the poorly constrained modern channel boundaries, suggesting insufficient flow in the ephemeral stream system to cause valley-wide channel migration, whether gradationally or by discrete jumps. Therefore, Sand Creek has not shown signs of valley-wide migration since the flow regime change, and the location of Sand Creek at the time of the Massacre in 1864 is concluded to be in the same location as the modern Sand Creek.

Conclusion

High Plains ephemeral stream migration and depositional processes were investigated using geophysical methods at Sand Creek, an ephemeral stream in Sand Creek Massacre National Historic Site. The results were used to determine whether Sand Creek has changed position since the Sand Creek Massacre in 1864, as historical documents describe events that occurred during the massacre with reference to their location relative to the stream. Four distinct layers are identified in the seismic refraction data: a thin layer that is 1 - 3 m thick with a velocity of 0.3 km/s and interpreted to be eolian sand; a gradational velocity layer that is 2 - 3 m thick with velocities ranging from 0.5 - 1 km/s, interpreted to be ephemeral channel alluvium deposits;

another gradational layer that is 2 - 7 m thick with velocities ranging from 1.2 - 2.9 km/s, interpreted to be perennial channel alluvium deposits that fill incised channels on top of the Pierre Shale Formation, which is the final refraction layer with a velocity of 2.4 km/s. The radar data reveal a change in bedforms at 3 - 4 m deep, which indicates a fluvial regime change from perennial to ephemeral flow. The initial period of perennial fluvial activity is revealed in the refraction data, as noted by channel incision into the Pierre Shale. Perennial fluvial sediments, including cobble-sized channel lag, fill these incised channels, as evidenced by diffractions mapped with the GPR data. In contrast, ephemeral stream deposits on top of the perennial fluvial sediments reveal laterally accreting and/or aggrading toplapping and downlapping horizons that correspond to distinct floods. These horizons are bounded within the wide, poorly constrained modern channel, indicating that ephemeral streams do not migrate across the valley bottom but rather have sub channels that flow within the modern channel boundaries during floods. Therefore, it can be concluded that the ephemeral Sand Creek has not migrated since the time of Sand Creek Massacre, but has had multiple depositional events within the modern channel.

References

Bridge, J., Collier, R., and Alexander, J., 1998, Large-scale structure of Calamus River deposits (Nebraska, USA) revealed using ground-penetrating radar: Sedimentology, v. 45, p. 977–986, doi: 10.1046/j.1365-3091.1998.00174.x.

Coffin, D.L., and Horr, C.A., 1967, Geology and ground-water resources of the Big Sandy Creek Valley, Lincoln, Cheyenne, and Kiowa Counties, Colorado; with a section on Chemical quality of the ground water:.

Earth System Research Laboratory (ESRL), Colorado Climate Division 1., 2005, SAND Annual & Monthly Climate Data:.

Graf, W.L., 1988, Fluvial Processes in Dryland Rivers (D. Barsch, I. Douglas, F. Joly, M. Marcus, & B. Messerli, Eds.): Berlin, Springer - Verlag.

Hirsch, M., Bentley, L.R., and Dietrich, P., 2004, A Comparison of Electrical Resistivity , Ground Penetrating Radar and Seismic Refraction Results at a River Terrace Site: Journal of Environmental & Engineering Geophysics, v. 13, p. 325–333.

Holmes, A., and Mcfaul, M., 1999, Geoarcheology Assessment, Laramie Soils service, Laramie WY:.

Lukas, J., and Woodhouse, C., 2006, Riparian Forest Age Structure and Past Hydroclimatic Variability, Sand Creek Massacre National Historic Site:.

Martin, M., Noon, K., and Biggam, P., 2013, Geomorphic and Hydrologic Assessment of the Historic Channel Position of Big Sandy Creek through Sand Creek Massacre National Historic Site, Colorado.:.

National Park Service, 2000, Denver, Intermountain region. Sand Creek Massacre Project, Site Location Study, v.1:.

Schrott, L., and Sass, O., 2008, Application of field geophysics in geomorphology: Advances and limitations exemplified by case studies: Geomorphology, v. 93, p. 55–73, doi: 10.1016/j.geomorph.2006.12.024.

SeisImager Manual, 2009, v 3.3, Geometrics, San Jose, CA

Sinha, R., Yadav, G.S., Gupta, S., Singh, A., and Lahiri, S.K., 2013, Geo-electric resistivity evidence for subsurface palaeochannel systems adjacent to Harappan sites in northwest India: Quaternary International, v. 308-309, p. 66–75, doi: 10.1016/j.quaint.2012.08.002.

Skelly, R.L., Bristow, C.S., and Ethridge, F.G., 2003, Architecture of channel-belt deposits in an aggrading shallow sandbed braided river: The lower Niobrara River, northeast Nebraska:

Sedimentary Geology, v. 158, p. 249–270, doi: 10.1016/S0037-0738(02)00313-5.

Słowik, M., 2011, Reconstructing migration phases of meandering channels by means of ground-penetrating radar (GPR): the case of the Obra River, Poland: Journal of Soils and Sediments, v. 11, p. 1262–1278, doi: 10.1007/s11368-011-0420-x.

Tooth, S., 2013, Dryland Fluvial Environments: Assessing Distinctiveness and Diversity from a Global, *in* Wohl, E. ed., Treatise on Geomorphology, Fort Collins, Co, Elsevier, p. 612–644.

USGS, 2005, Arkansas River Basin, Big Sandy Creek Streamflow: Colorado Water Science Center.

Vandenberghe, J., and Overmeeren, R.A. Van, 1999, Ground penetrating radar images of selected fluvial deposits in the Netherlands: Sedimentary Geology, v. 128, p. 245–270, doi: 10.1016/S0037-0738(99)00072-X.

Wooldridge, C.L., 2005, Radar Architecture and Evolution of Channel Bars in Wandering Gravel-Bed Rivers: Fraser and Squamish Rivers, British Columbia, Canada: Journal of Sedimentary Research, v. 75, p. 844–860, doi: 10.2110/jsr.2005.066.

CHAPTER 3: ADDITIONAL FIGURES AND FILES

Introduction

This chapter contains supplementary figures for the figures included in Chapter 2. The field topography, seismic, and GPR data, processing stream, and final data products are digitally archived and can be accessed by anyone using this link: Brad Sparks Thesis Data Files or by emailing cubsdolphinfan@gmail.com and requesting a zipped folder.

Seismic Survey Data and Figures

The complete seismic dataset consists of over 200 shot records, which are contained in the archive files described above. Typical shot records are shown representing poor data (Figure 1 - less than 5% of my seismic data was this quality), average data (Figure 2 - about 55% of my data was this quality), and optimal data (Figure 3 - about 40% of my data was this quality).

First break picks and travel time plots, with the interpreted layer assignments, are shown in Figures 1 – 3 and correspond to the cases of poor, average, or optimal data quality. Final tomographic inversions for each profile are also shown in Figures 1 – 3 also corresponding to the cases of poor, average, and optimal data quality.

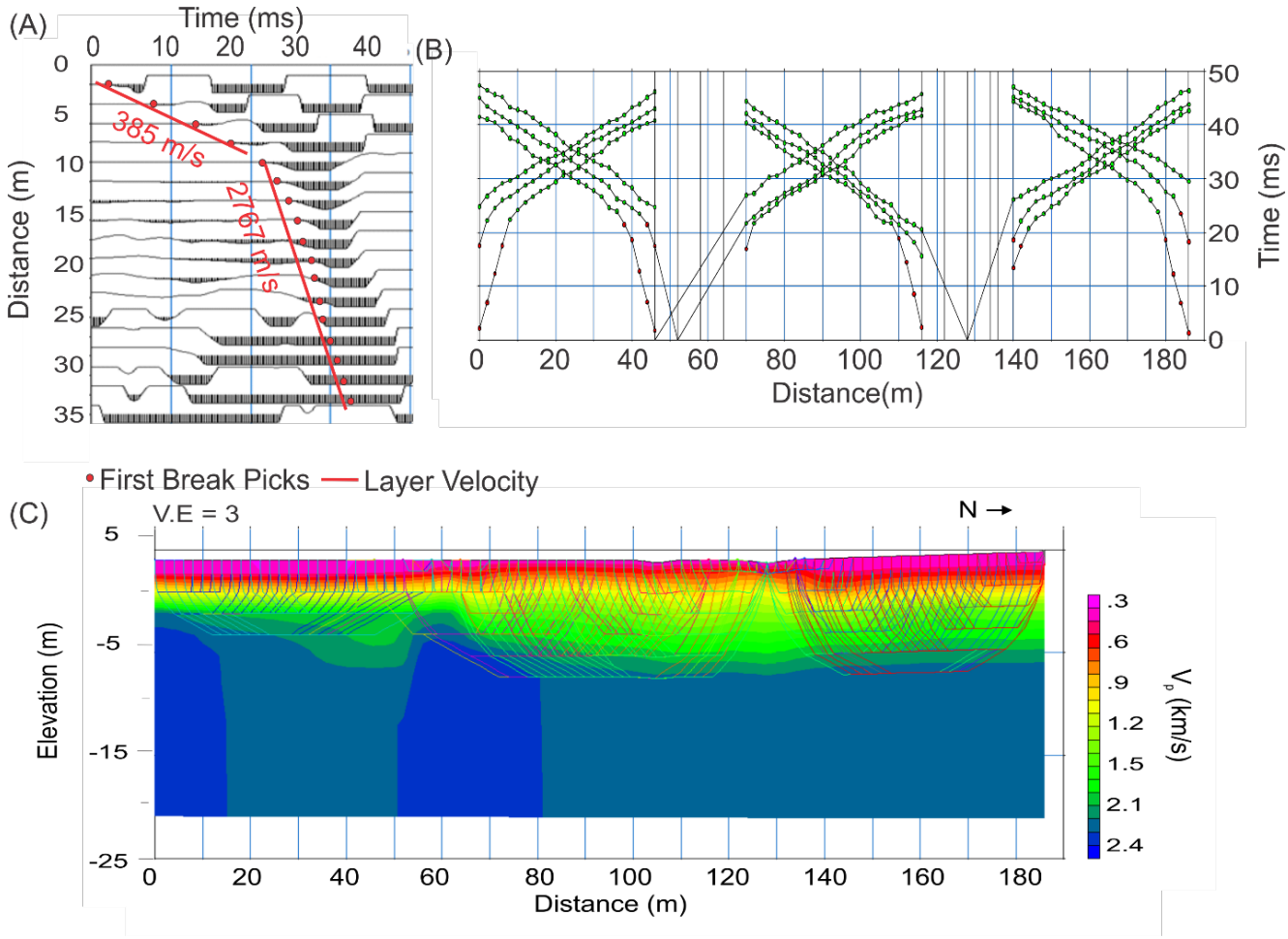

Figure 16. An example of poor data quality for a seismic survey, from Line 3. (A) Shows the first break picks and velocity for both layers. (B) Shows the assignments for the two velocity layers. (C) Shows the tomography model with the raypaths showing the interrogated areas.

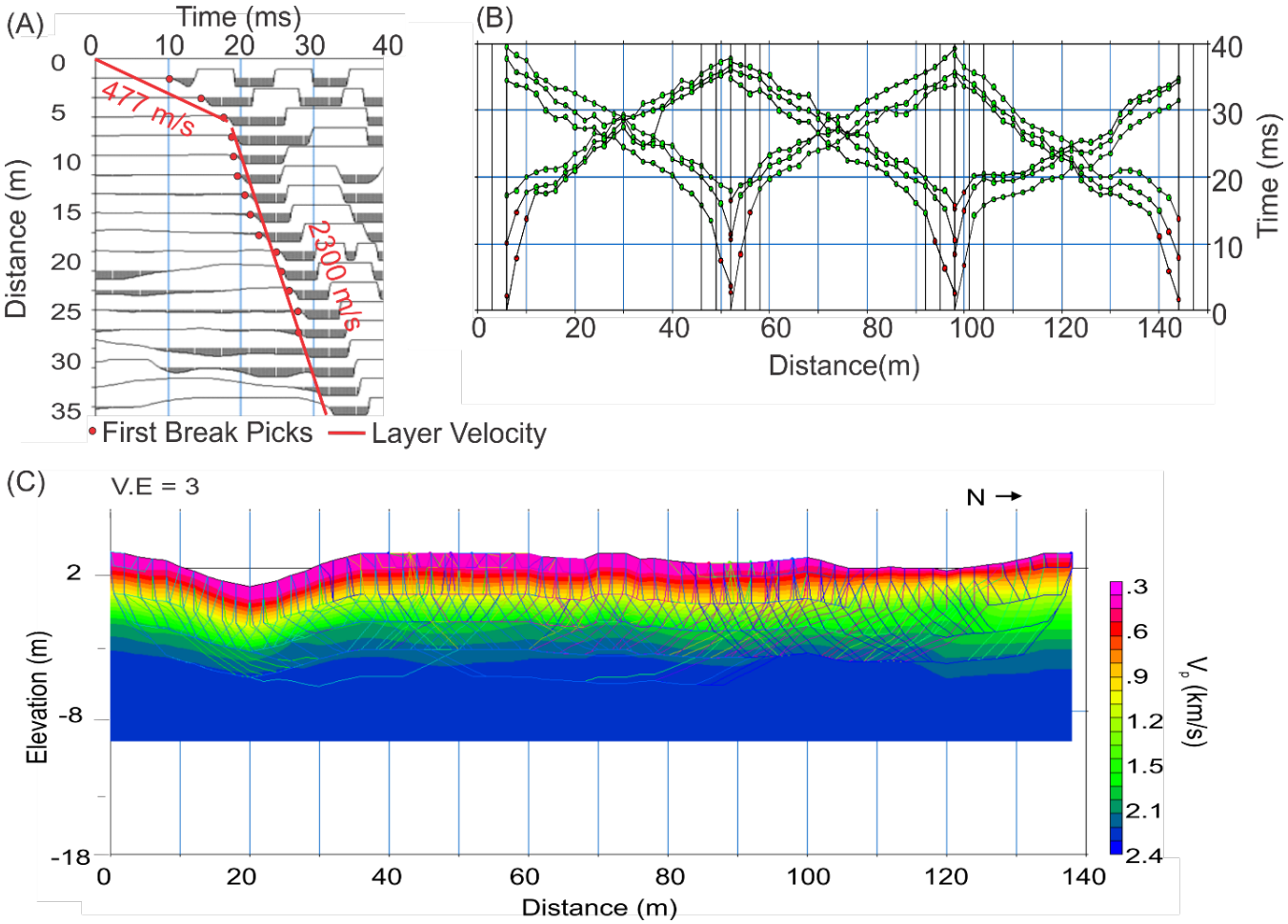

Figure 17. An example of average data quality for a seismic survey, from Line UP2. (A) Shows the first break picks and velocity for both layers. (B) Shows the assignments for the two velocity layers. (C) Shows the tomography model with the raypaths showing the interrogated areas.

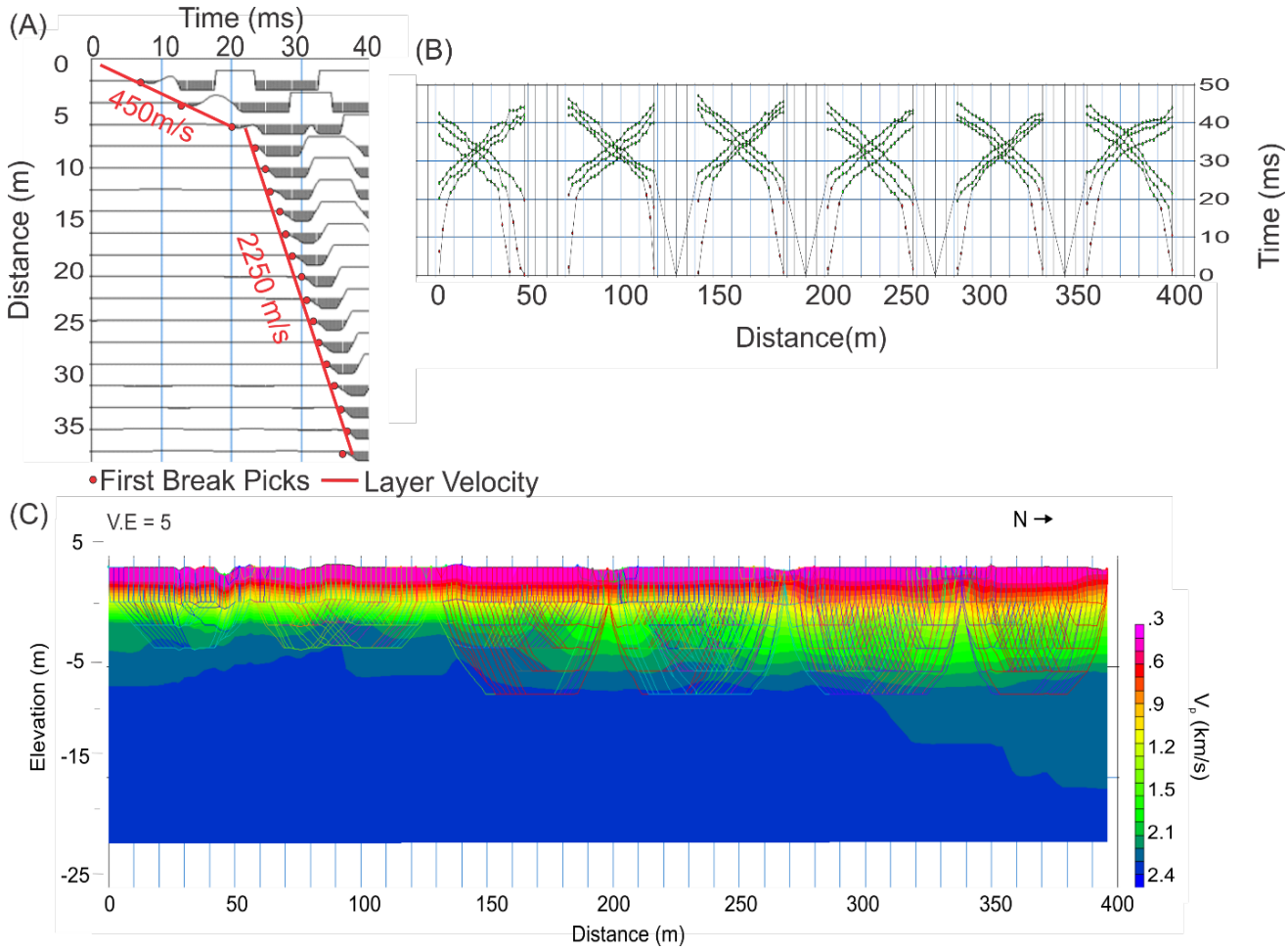

Figure 18. An example of optimal data quality for a seismic survey, from Line 1. (A) Shows the first break picks and velocity for both layers. (B) Shows the assignments for the two velocity layers. (C) Shows the tomography model with the raypaths showing the interrogated areas.

CHAPTER 4: RECOMMENDATIONS FOR FUTURE RESEARCH

Introduction

This chapter provides suggestions for further research as well as pragmatic advice for anyone undertaking future research regarding Sand Creek. The following text was a product of my experience working over the span of 2 years taking long drives down to Eads, Colorado; working in the field at the National Historic Site; and spending hours in the lab processing data and fixing equipment.

Further Research Ideas

While researching at Sand Creek I was limited by time and manpower, so I never got the opportunity to explore some ideas I found interesting that were ancillary to my research. Those research ideas were:

- Taking valley wide lines and grids of GPR data to recreate the history of the valley drainage as a whole. A 3D model that displayed what the past flow regime looked like would have been a fascinating outcome.
- Conducting GPR and Refraction surveys a few miles upstream and downstream and comparing the results to determine the connectivity of Sand Creek flows.
- Utilizing more coring to augment GPR and seismic results, especially in places where significant bedforms were imaged.
- Systematically Surveying Sand Creek up to its headwaters to better understand the entire stream process.